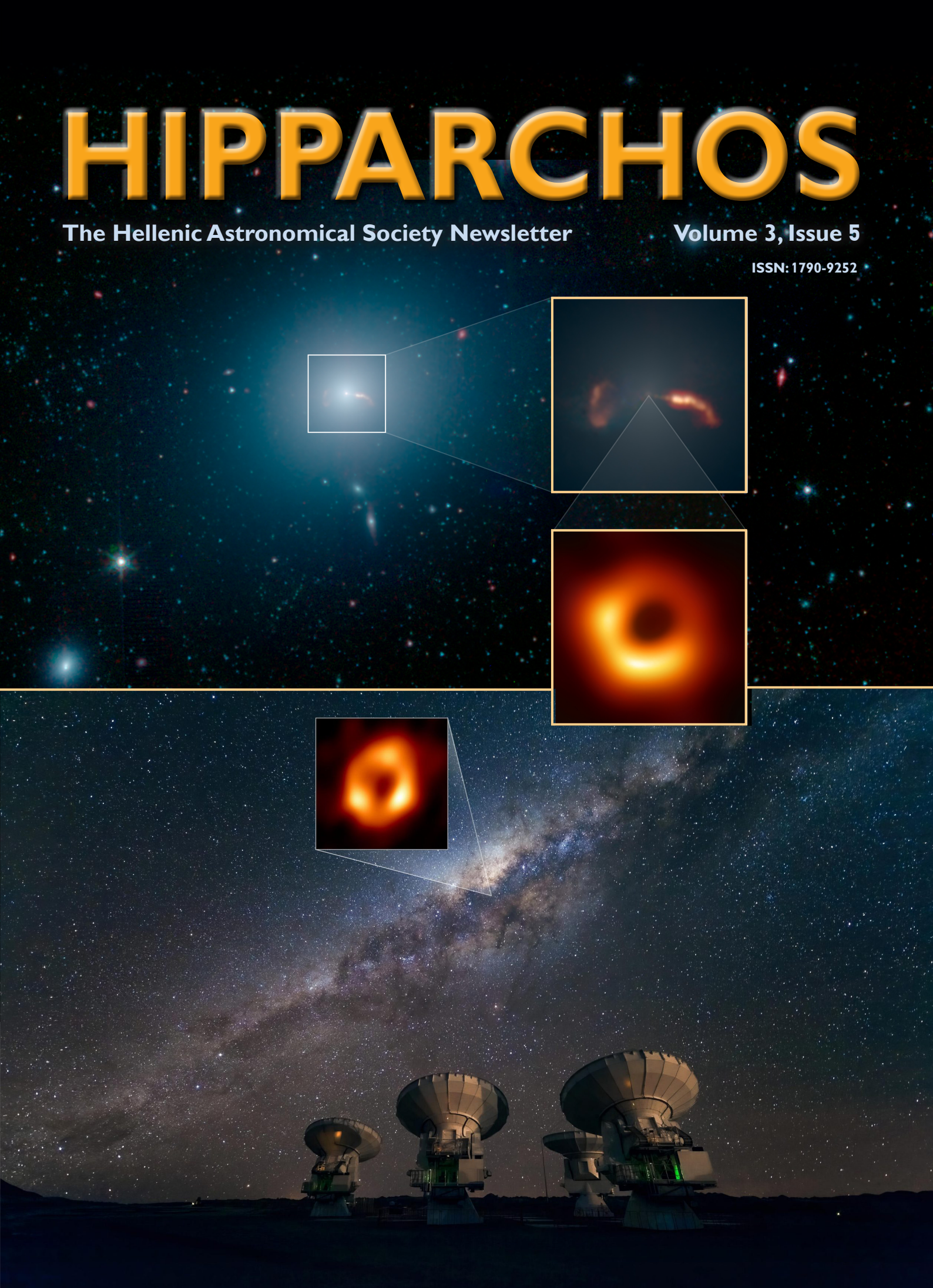


# HIPPARCHOS

The Hellenic Astronomical Society Newsletter

Volume 3, Issue 5

ISSN: 1790-9252





# Contents

**HIPPARCHOS**

Volume 3, Issue 5 • July 2022

ISSN: 1790-9252

Hipparchos is the official newsletter of the Hellenic Astronomical Society. It publishes review papers, news and comments on topics of interest to astronomers, including matters concerning members of the Hellenic Astronomical Society.

## Editorial board

- **Kostas Gourgoulis**  
(Physics Dept., University of Patras)
- **Spiros Patsourakos**  
(Physics Dept., University of Ioannina)
- **Kostas Tassis**  
(Physics Dept., University of Crete)
- **Nektarios Vlahakis**  
(Physics Dept., University of Athens)

## Contact person

Nektarios Vlahakis  
Physics Department, National and Kapodistrian University of Athens,  
University Campus,  
157 84 Zografou,  
Athens, Greece  
Tel: +30-210-7276903  
E-mail: vlahakis@phys.uoa.gr

## Editorial Advisors

- **Vassilis Charmandaris**  
(Physics Dept., University of Crete)
- **Antonios Georgakakis**  
(National Observatory of Athens)
- **Costis Gontikakis**  
(RCAAM, Academy of Athens)

Printed by ZITI Publications • www.ziti.gr

**Message from the President** ..... 3

## REVIEWS

**A new ( $\nu$ ) view of blazar jets**  
by Maria Petropoulou ..... 4

**The Extreme Environments of Luminous Infrared Galaxies**  
by Tanio Díaz-Santos ..... 11

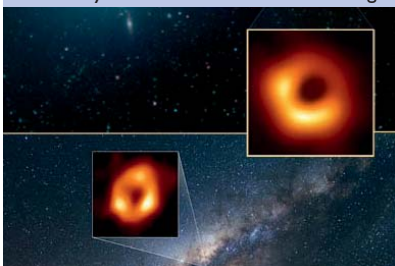
**Semi-empirical modelling of the Energetic Universes**  
by Antonis Georgakakis and Ivan Muñoz Rodríguez ..... 17

**Revisiting star and planet formation in the era of Big Data**  
by Odysseas Dionatos ..... 22

**Historical developments**  
by George Contopoulos ..... 28

## CONFERENCES

**COSPAR's 44th Scientific Assembly in Athens:  
a first for Greece at a historic juncture**  
by Manolis K. Georgoulis ..... 31



### Cover Images:

Top: This wide-field image of the galaxy M87 was taken by NASA's Spitzer Space Telescope. The top inset shows a close-up of two shockwaves, created by a jet emanating from the galaxy's supermassive black hole. The second inset shows that black hole imaged by the Event Horizon Telescope (EHT).  
Credit: NASA/JPL-Caltech/EHT Collaboration.

Bottom: This image shows the Atacama Large Millimeter/submillimeter Array (ALMA) looking up at the Milky Way as well as the location of Sagittarius A\*, the supermassive black hole at our galactic center. Highlighted in the box is the image of Sagittarius A\* taken by the EHT.  
Credit: ESO/José Francisco Salgado (josefrancisco.org), EHT Collaboration.

# Message from the President



**W**hen in the May 2021 I was writing my first message to all members of HelAS as the President of the Society, we were all in the middle of the pandemic that was affecting our lives greatly. Our Society, like many others, was forced to plan its first virtual Conference in July 2021. Despite the difficulties, thanks to the hard work of everyone involved and the flexibility of the remote presence, the 15<sup>th</sup> Hellenic Astronomical Conference was attended by 227 participants from 24 countries, making it the most popular of all conferences the Society has organized so far. The science program was rich, the presentations of excellent quality, and the discussions very lively. Moreover, all talks and nearly all poster presentations became available online in the YouTube Channel of the Society for everyone to peruse at their own leisure after the conference. I believe that this experience and the advances in technology will likely motivate us to explore the possibility of organizing the future conferences of our Society in a hybrid mode.

Time flies though, another year has passed, and the term of the current Governing Council of the Society is coming to an end. Four members of the Council, Dr. Antonis Georgakakis, Dr. Costis Gontikakis, Prof. Spiros Patsourakos, and Prof. Nektarios Vlahakis, completed their two terms at the office and are stepping down. On behalf of all of us I would like to express our gratitude to them for the personal time, energy and creative ideas they offered to the Society in order to improve its services to all members, as well as fulfill in the best way possible its mission.

The new members of the Council and the Auditors will be elected on June 24, 2022 the day of our 41<sup>st</sup> General Assembly using for the first time an electronic voting system. This possibility is only feasible thanks to the modifications to the Constitution of the Society, which were formally approved by the court of Athens in January 2022. The system we will use is “ZEUS” of GRNET, which is being used by all academic institutions in Greece for many years. In May 2022 the Council and the Elections Committee tested the system successfully and we are all optimistic that the election process will run smoothly. We also hope that the convenience of the online voting will not only reduce the financial cost and heavy administrative load of the elections, but it will also encourage more members of the Society to actively participate in them.

Over the past year, the Society continued the organization of the monthly colloquia by selecting high quality speakers from across the globe. The presentations were excellent even though the participation was not as high as one would have liked given the size of our Society. This could be due to fatigue of too many online meetings, as well as to the actual time the colloquia were taking place, which at 6pm Athens’ time, was outside the normal business hours in Greece. I expect that the new Council will take actions to evaluate and remedy the situation. Moreover, the Society continued to support the public outreach activities of a dynamic group of Junior Members, who established the “2 minute Science”, as well as the “Hel.A.S. NextGen Seminar Series”. These semi-

nars offer to members of our Society at the early stage of their career, such as PhD students and postdoctoral researchers, the opportunity to obtain valuable experience by presenting their research work in front of an audience.

The Vice Chair of the Society, Prof. Nektarios Vlahakis, was also responsible to select and edit several invited articles on pertinent areas of astrophysics, which appear in the present issue of Hipparchos. Prof. Maria Petropoulou is presenting the latest results on the physics of Blazars and their neutrino emission, Dr. Tanio Diaz Santos is writing about his work on the extreme environments of Luminous Infrared Galaxies, while Dr. Antonis Georgakakis and Dr. Ivan Muñoz Rodríguez brief us on the latest progress on semi-empirical modelling of the Energetic Universe. All three articles are related to research proposals of the authors that have been recently funded by the Hellenic Foundation for Research and Innovation. In addition, Dr. Odysseas Dionatos sheds new light on our understanding of star and planet formation in the era of Big Data, while Prof. George Contopoulos, the Honorary President of our Society, is sharing with us a historical perspective on the existence of closed invariant KAM curves and on infinite bifurcations. Finally, Dr. Manolis Georgoulis will tell us what to expect during the COSPAR meeting, which takes place in Athens in July.

I am certain that we will enjoy and learn a lot by reading all those articles carefully!

---

*Vassilis Charmandaris*  
*President of Hel.A.S.*

---

# A new ( $\nu$ ) view of blazar jets

by Maria Petropoulou

Department of Physics, National and Kapodistrian University of Athens, Greece

## 1. Blazars in a nutshell

Active galactic nuclei, or AGN for short, are galaxies with bolometric luminosities  $10^{43}$ - $10^{48}$  erg s<sup>-1</sup> whose central nucleus outshines the rest of the galaxy [for a review, see Padovani et al., 2017]. To better grasp these numbers, let us consider that the energy released by an AGN in just one second is equivalent to the energy released by our Sun in ~3,000 years! AGN are believed to be powered by a spinning black hole whose mass is millions up to billions times larger than the mass of our Sun. While in “normal” galaxies, like our Milky Way, the supermassive black hole (SMBH) is dormant, in AGN is being constantly “fed” with matter forming a disk. As the material moves inward toward the black hole, tremendous amounts of gravitational energy are released and transformed into other forms of energy, including heat and thermal radiation. The accreting SMBH is practically the powerhouse of an AGN.

Roughly 10% of AGN produce highly collimated outflows of magnetized plasma, called jets, that move with relativistic speeds away from the central engine, as illustrated in Fig. 1. It is commonly accepted that the energy source of jets is the spinning black hole itself (Blandford-Znajek process) [Blandford & Znajek, 1977] or the inner accretion disk threaded by large-scale poloidal magnetic fields (Blandford-Payne mechanism) [Blandford & Payne, 1982]. In both scenarios, the magnetic field extracts rotational energy and momentum outwards in the form of a magnetically dominated jet. At a certain distance within the jet, which still remains uncertain, the magnetic energy of the jet is converted to energy of relativistic particles that eventually produce the non-thermal radiation we observe [for an overview, see Rani et al., 2019].

Blazars are a subclass of AGN with jets pointing almost directly to us! Because of their relativistic motion, which can actually be observed at GHz frequen-



**Figure 1:** Artist's impression of a blazar: a galaxy powered by a supermassive black hole, which produces powerful jets of magnetized plasma pointing directly to Earth. Blazars are among the brightest objects in  $\gamma$ -rays, the most energetic photons detected. (Credit: M. Weiss/CfA)

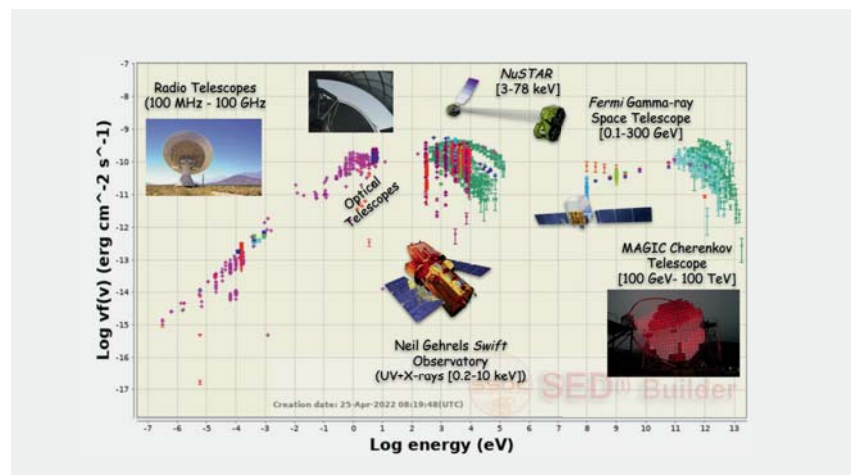


**Figure 2:** Spectral energy distribution (SED) of Mkn 421, the nearest blazar to Earth, compiled from archival data (<https://tools.ssdc.asi.it/SED/>) spanning 20 orders of magnitude in energy. High-energy (X-ray and  $\gamma$ -ray) emission is strongly variable on various time-scales (e.g. hours to weeks). Examples of observatories involved in the study of blazars are also overplotted.

cies in real human time<sup>1</sup>, the non-thermal jet radiation will appear Doppler boosted<sup>2</sup>, and will dominate the emission coming from regions external to the jet (e.g., from the accretion disk or from clouds in the broad line region, BLR). *Electromagnetic observations of blazars are therefore probing physical processes that take place*

*at the extreme conditions of relativistic jets.* Blazars are characterized by flux variability (i.e., fluctuations away from an average value) that is frequency-dependent and manifests in a variety of timescales, ranging from years to a few minutes. To put things into perspective, ~8 minutes is the time a photon needs to cross a region with size equal to the gravitational radius of a SMBH with mass 100 million times the mass of the Sun! The spectral energy distributions (SEDs) of blazars generally show two broad components (or humps) that span ~15 decades in energy, from ra-

1. <http://www.astro.purdue.edu/MOJAVE/>  
2. The Doppler factor of a source moving with Lorentz factor  $\Gamma > 1$  at an angle  $\theta$  with respect to the line of sight is defined as  $D = \Gamma^{-1}(1 - \beta \cos \theta)^{-1} \approx \Gamma$  for small angles. The bolometric luminosity in the observer's frame,  $L$ , is related to the luminosity in the jet rest-frame,  $L'$ , as  $L = D^4 L'$ .

dio frequencies up to very high-energy (VHE)  $\gamma$ -rays (see e.g., Fig. 2). Blazars are also classified into three spectral subclasses depending on the peak energy of their low-energy hump [Abdo et al., 2010]: high-peaked energy sources (HBL/HSP,  $E_{\text{peak}} > 4.1$  eV), intermediate-peaked energy sources (IBL/ISP,  $0.41$  eV  $< E_{\text{peak}} < 4.1$  eV), and low-peaked energy sources (LBL/LSP,  $E_{\text{peak}} < 0.41$  eV). It is well established that the low-energy component, extending from radio frequencies to X-ray energies, is produced by the synchrotron emission of relativistic electrons and positrons accelerated in the jet. *However, the origin of the high-energy component, extending from X-rays to  $\gamma$ -rays, is still debatable* [for a review, see Böttcher, 2019].

## 2. High-energy radiation models

The first extragalactic source to be discovered in  $\gamma$ -rays ( $> 100$  MeV) was blazar 3C 273 by the COS-B satellite in the late 70s [Swanenburg et al., 1978]. But it was not until the 90s, after the detection of tens of blazars in  $\gamma$ -rays by EGRET, that the interest in high-energy processes in blazars got its boost [e.g., Hartman et al., 1999]. EGRET made two unexpected discoveries: (i) in the majority of blazars, the  $\gamma$ -ray emission dominates the bolometric power in their SED, and (ii) the  $\gamma$ -ray emission is variable on time-scales of the order of days to months. Nowadays it is common knowledge that  $\gamma$ -rays are an integral part of relativistic jet emission. In fact, blazars have been shown to contribute  $\sim 50\%$  to the total extragalactic  $\gamma$ -ray background (EGB) and almost 100% above 100 GeV [e.g., Ajello et al., 2015]. These findings were made possible thanks to the *Fermi*  $\gamma$ -ray telescope that has been in operation since 2008, and surveys the sky in the 0.1–300 GeV range every  $\sim 3$  hrs<sup>3</sup>.

Various theoretical models about the high-energy blazar emission have been developed in the years following the EGRET detections. These can broadly be divided into two classes based on the particle species radiating in  $\gamma$ -rays, namely *leptonic models* and *hadronic models*. In the former class, the high-energy component of the SED is explained by inverse Compton scatter-

ing (ICS) of soft photons by relativistic electrons accelerated in the jet (primary electrons). The seed photons for ICS can be the synchrotron photons produced by the same electron population [synchrotron self-Compton (SSC) models, see e.g., Maraschi et al., 1992; Mastichiadis & Kirk, 1997] or from an external region, such as the accretion disk (AD) or the BLR [external Compton (EC) models, see e.g., Dermer et al., 1992; Sikora et al., 1994]. For a schematic illustration of the inner blazar environment, see Fig. 3. The processes responsible for accelerating electrons to relativistic energies (e.g., shock acceleration, magnetic reconnection and others) are expected to act also on hadrons. In fact, these can reach much higher energies than electrons, because they are not as strongly affected by radiative losses. Jetted AGN are one of the few astrophysical environments that can confine the highest energy ( $\sim 10^6 - 10^8$  TeV) protons and heavier ions that we detect on Earth as ultra-high-energy cosmic rays [Hillas, 1984]. If the power carried by relativistic hadrons in the jet is sufficiently high, then their radiation cannot be neglected, thus motivating hadronic emission models.

Because the blazar environment is rich in radiation fields and the thermal plasma density of the jet is low, special attention was given to photohadronic in-

teractions (inelastic collisions of protons with low-energy photons) as means of producing high-energy radiation. Photohadronic interactions are comprised of two processes of astrophysical interest, namely

- photopair (pe) production (Bethe-Heitler) process:  
 $p + \gamma \rightarrow p + e^- + e^+$
- photomeson (p $\pi$ ) production process:  
 $p + \gamma \rightarrow \Delta^+ \rightarrow n + \pi^+, \pi^+ \rightarrow \mu^+ + \nu_\mu$   
 $\mu^+ \rightarrow e^+ + \bar{\nu}_\mu + \nu_e$  or  
 $p + \gamma \rightarrow \Delta^+ \rightarrow p + \pi^0, \pi^0 \rightarrow 2\gamma$

Both processes inject into the jet relativistic electrons and positrons, but only the second mechanism produces neutrinos. These are standard model particles that are neutral and almost massless; the most stringent upper limit on their mass is 0.8 eV/ $c^2$  [Katrin Collaboration et al., 2022], to be compared with the electron rest mass of 511 keV/ $c^2$ . They are very hard to detect, because they interact with matter very weakly. To appraise the latter just consider that about 100 billion neutrinos are passing through your thumb every second without even noticing it!

The target photons needed for photohadronic interactions could have an external origin, as in leptonic EC models

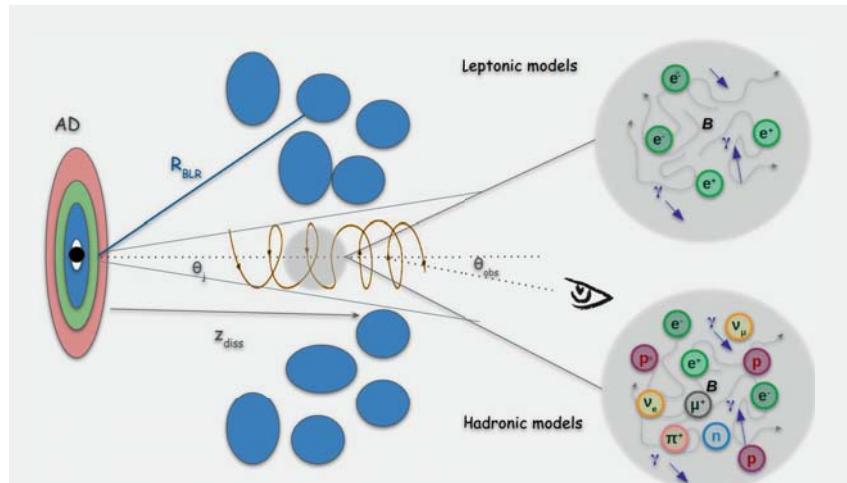


**Figure 3:** Schematic illustration of the inner parsec regions of a blazar (not to scale). A jet – collimated outflow of magnetized plasma – is launched from a spinning black hole that is accreting material through a multi-temperature accretion disk (AD). The disk illuminates dense clouds of gas (blue colored blobs) from the broad line region (BLR) that re-emit thermal radiation almost isotropically. At a some distance from the black hole,  $z_{\text{diss}}$ , particles accelerate to relativistic energies producing non-thermal radiation, received by an observer at a small angle ( $\theta_{\text{obs}} \sim 5^\circ$ ). In *leptonic models* the emitting region contains magnetic fields ( $B$ ), photons ( $\gamma$ ) and pairs ( $e^-e^+$ ). In *hadronic models*, it contains additionally protons ( $p$ ), which produce unstable particles, like pions ( $\pi^\pm, \pi^0$ ). These eventually produce more pairs and neutrinos ( $\nu_\mu, \nu_e$ ).

3. <https://www.nasa.gov/content/fermi-gamma-ray-space-telescope>

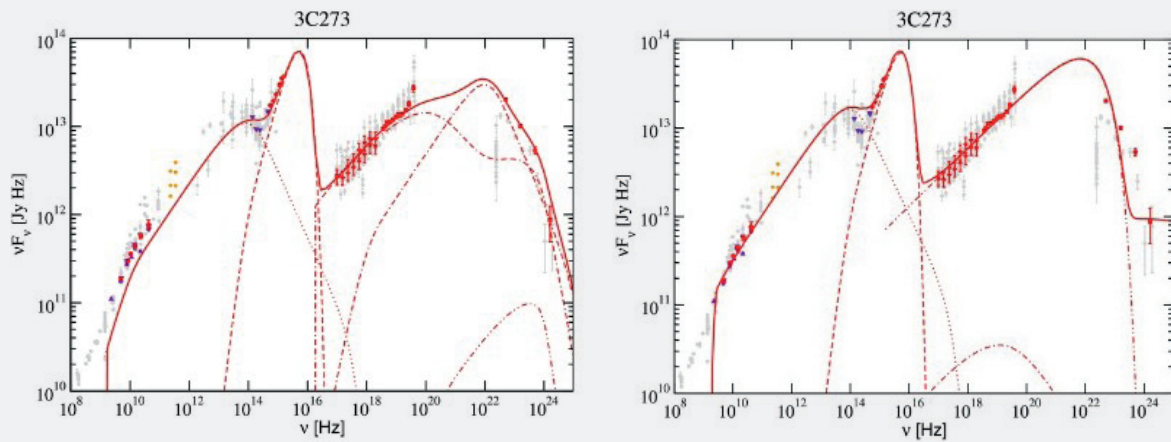


**Figure 4:** Leptonic EC model (left) and hadronic PS model (right) fits to multi-wavelength observations of blazar 3C 273 (colored symbols). Dotted: electron-synchrotron; dot-dashed: SSC; dashed: AD; dot-dash-dashed: EC (AD); dot-dot-dashed: EC (BLR) for the leptonic model, and proton-synchrotron for the hadronic model (figure from Böttcher et al. [2013]; reproduced by permission of the AAS).

[e.g., Atoyan & Dermer, 2001; Bednarek & Protheroe, 1999], or they could be produced in the jet by the co-accelerated electrons, as in SSC models. The high-energy component of the SED in hadronic scenarios may have different origins. For instance, it can be produced:

- *directly* by protons through synchrotron radiation [PS models, e.g., Mücke & Protheroe, 2001], or
- *indirectly* through the decay of neutral pions [e.g., Sahu et al., 2013], or through synchrotron and Compton processes of secondary pairs produced in  $pe$ ,  $p\pi$  or  $\gamma\gamma$  pair production processes; these are known as the proton-initiated cascade (PC) models [e.g., Mannheim, 1993; Petropoulou et al., 2015].

Various studies within the last decade have demonstrated that leptonic and hadronic models describe equally well the average broadband emission of a handful of well monitored sources (see e.g., Fig. 4), yet implying very different jet energetics and physical conditions in the emitting region. Nonetheless, SED modeling alone cannot convincingly rule out one of the two scenarios [Böttcher, 2019]. Unraveling the origin of the high-energy radiation of blazars (i.e., leptonic versus hadronic) is of paramount importance for understanding the physics of jets in general (e.g., baryon loading mechanisms, jet launching and energetics). *Detection of high-energy neutrinos from blazars would be the smoking gun of the presence of relativistic hadrons in relativistic jets.*

### 3. The dawn of neutrino astrophysics

Till recently the only known extraterrestrial neutrino sources were the Sun and SN 1987A in the Large Magellanic Cloud. In 2013 the IceCube Neutrino Observatory<sup>4</sup> announced the discovery of an astrophysical high-energy (10 TeV–10 PeV) neutrino flux [Aartsen et al., 2013a,b], opening a new window to the energetic Universe.

The origin of these neutrinos remains still a mystery.

No strong steady [Aartsen et al., 2017a] or variable neutrino point sources, or a neutrino correlation with the Galactic plane has been identified in the IceCube data [Aartsen et al., 2015, 2019; Albert et al., 2018].

This suggests that a large population of extragalactic sources, such as blazars and non-jetted AGN, could be responsible for the bulk of the diffuse neutrino flux [for a recent review, see Murase & Stecker, 2022].

The contribution of blazars to the diffuse neutrino flux has experimentally been constrained to the level of ~10-30% by correlation and stacking analyses [Aartsen et al., 2017b; Murase et al., 2018]. Meanwhile, theoretical models for the diffuse neutrino flux from the blazar population usually predict spectra peaking at ultra-high-energies (UHE, > 10 PeV) [e.g., Padovani et

al., 2015], and are constrained by the Ice-Cube UHE non-detections [Aartsen et al., 2018].

The fact that blazars are not the dominant contributors to the bulk of the diffuse neutrino flux does not mean that they cannot be detected as *neutrino point sources*. The first compelling evidence for the identification of an astrophysical high-energy neutrino source was provided in 2017 by the detection of a > 290 TeV neutrino (IC 170922A) in coincidence with an energetic  $\gamma$ -ray flare from the blazar TXS 0506+056 [Aartsen et al., 2018a], as illustrated in Fig. 5. A follow-up analysis of archival IceCube neutrino data revealed a “neutrino excess” during a ~100-day window in 2014/15 [Aartsen et al., 2018b], which however was not accompanied by flaring in  $\gamma$ -rays Garrappa et al. [2019].

### 4. Current status of the field

The unique data set of the 2017 flare of TXS 0506+056 motivated many theoretical studies of its multi-messenger emission [e.g., Cerruti et al., 2019; Gao et al., 2019; Keivani et al., 2018]. Contrary to expectations, SED modeling of TXS 0506+056 showed that the broadband photon spectra cannot be explained concurrently with the detection of one high-energy neutrino, if hadronic processes dominate the  $\gamma$ -ray band. Either the neutrino flux is too low or the photon emission overshoots the X-ray observations (compare dashed and solid lines in top panel of Fig. 6).

4. This is a cubic-kilometer particle detector made of ice, located in Antarctica. It is buried beneath the surface, extending to a depth of about 2.5 km (<https://icecube.wisc.edu/science/icecube/>).

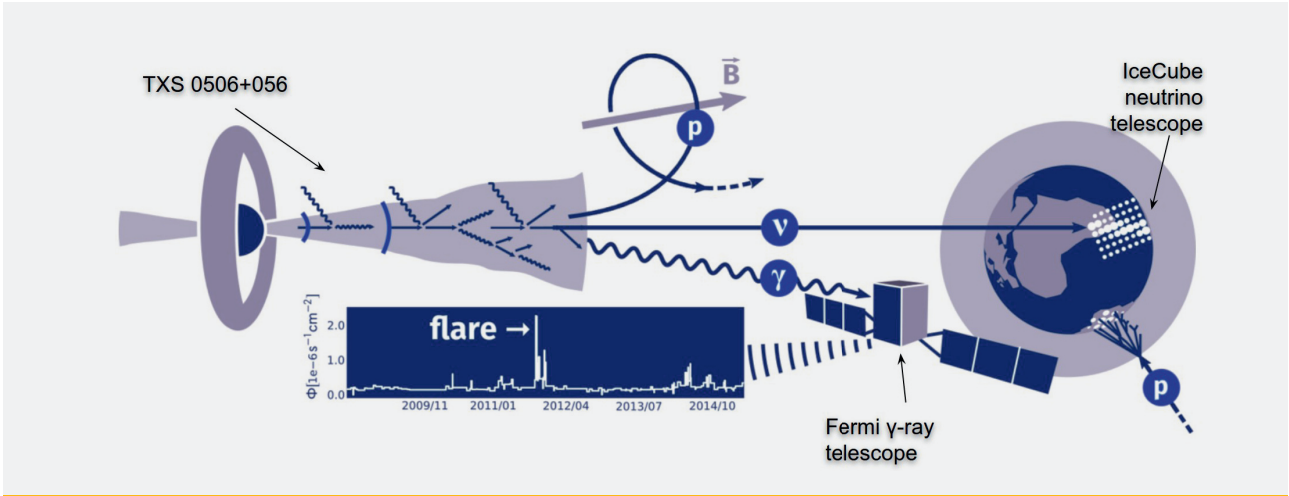


**Figure 5:** Schematic illustration of high-energy neutrino detection in spatial and temporal coincidence with a  $\gamma$ -ray flaring blazar, TXS 0506+056. To date, this is the only astronomical source significantly associated with high-energy neutrinos. Image credit: IceCube Collaboration (<https://www.iihe.ac.be/icecube>).

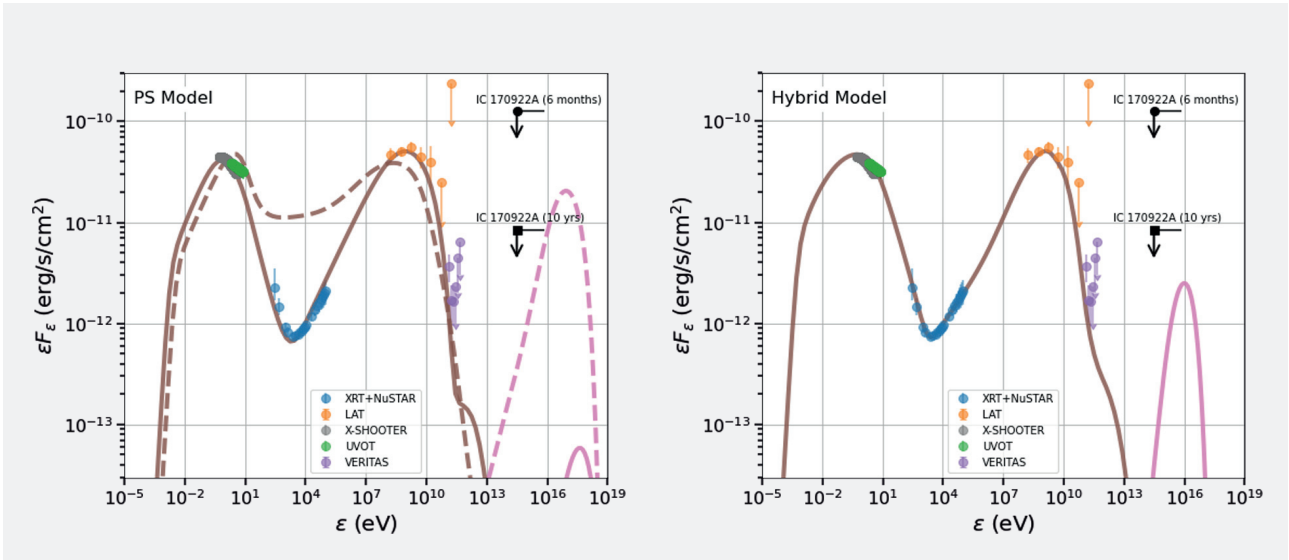


**Figure 6:** SED models for the 2017 flare of TXS 0506+056 from Keivani et al. [2018]. The predicted all-flavor neutrino spectrum is shown in pink. Overplotted as colored symbols are data from various instruments (see inset legend). Black arrows indicate the inferred neutrino fluxes from the detection of 1 neutrino, IC 170922A, for two assumed durations. *Left panel:* The PS model fails to produce a high neutrino flux without overshooting the X-ray data (dashed lines). *Right panel:* Contrary to expectations, the data can be explained by a *hybrid model* where the radiative signatures are hidden below the emission of co-accelerated electrons.

Instead, a leptonic scenario with a radiatively subdominant hadronic component (henceforth, *hybrid model*) provides the only physically consistent picture for this source's multi-messenger emission – see right panel in Fig. 6. According to this, protons are accelerated in the blazar jet to tens of PeV energies, carrying 200-500 times more power than co-accelerated electrons. Protons then pion-produce on jet synchrotron photons and weak external radiation fields, producing 0.1-1 PeV neutrinos. Under these conditions, the probability for IceCube to detect a neutrino like IC-170922A in real time during the blazar flare is about 2%.

The maximum neutrino flux allowed in this scenario can also be obtained using analytical arguments. These rely on the fact that the emission from proton-initiated cascades peaks in the X-ray and soft- $\gamma$ -ray bands (0.1-100 keV) for typical parameters, and is closely related to the neutrino emission. As a result, by the broadband X-ray luminosity [Murase et al., 2018],

$$E_\nu L_\nu(E_\nu) \leq \frac{3}{8} \left[ \frac{5}{16} + \frac{g(\beta)}{2} \right]^{-1} \frac{L_X}{f_X} \approx \quad (1)$$

$$\approx 10^{45} \left( \frac{L_X}{3 \times 10^{45} \text{ erg/s}} \right) \left( \frac{f_X}{0.1} \right)^{-1} \text{ erg/s}$$

where  $L_\nu(E_\nu)$  is the differential in energy neutrino luminosity,  $f_X$  is the fraction of the cascade emission that emerges in the X-ray band,  $L_X$  and  $\beta \sim 2.5$  are respectively the luminosity and photon index in the 0.3-10 keV energy band, and  $g(\beta) \approx 0.01 (30)^{\beta-1}$ .

The lack of an electromagnetic flare during the 2014/15 neutrino excess does not fit well in the above picture. The 6-month neutrino luminosity of TXS 0506+056 in the 0.1-1 PeV range was found to be about 4 times larger than the average  $\gamma$ -ray luminosity detected by *Fermi*-LAT. This translates to a neutri-

no flux of  $\sim 3 \times 10^{-11}$  erg cm $^{-2}$  s $^{-1}$ , which according to Eq. (1), should correspond to the average X-ray flux of the source. Such high fluxes would have been easily detected by X-ray monitoring instruments like *Swift* and MAXI, but both yielded upper limits.

#### 4.1 More flaring blazar - neutrino associations?

From an experimental point of view, neutrino searches during blazar flares (or other transients in general) are more sensitive because of the reduced background. From a theoretical standpoint, flares are generally speaking promising times for neutrino production. This can be understood qualitatively as follows. The all-flavor neutrino luminosity can be written as

$$E_\nu L_\nu(E_\nu) \approx \frac{3}{8} f_{p\pi}(E_p) E_p L_p(E_p) \quad (2)$$

where  $L_p(E_p)$  is the differential in energy proton luminosity,  $E_p$  is the proton energy, which relates to the neutrino energy as  $E_p \approx 20E_\nu$ , and  $f_{p\pi}$  is the so-called photopion efficiency. This quantity carries all the information about the opacity of the source in  $p\pi$  interactions, and as such it depends on parameters like the density and spectrum of target photons, the proton energy, and the cross section of the interaction [e.g., Murase et al., 2014],

$$f_{p\pi}(E_p) \approx \frac{2}{1 + \beta} \hat{\sigma}_{p\pi} \frac{L_{ph,s}}{4\pi R D^3 E_{ph,s}} \left( \frac{E_p}{E_{p,b}} \right)^{\beta-1} \quad (3)$$

Here,  $\hat{\sigma}_{p\pi} \approx 5.9 \times 10^{-29}$  cm $^2$  is the effective cross section of the interaction at the  $\Delta$  resonance,  $L_{ph,s}$  is the observed target photon luminosity,  $E_{ph,s}$  is the target photon energy,  $\beta$  is the photon index of the target photon spectrum,  $R$  and  $D$  are respectively the radius and Doppler factor of the emitting region, and  $E'_{p,b} \approx 0.17$  GeV $D^2 m_p c^2 / E_{ph,s}$ . During a flare, the proton and target photon luminosities can increase, hence leading to a non-linear increase of the neutrino flux, as suggested by Eqs. (2) and (3).

Since the observation of IC 170922A, more blazars have been found in the error circles of high-energy alert neutrinos, albeit with lower significance individually [Garrappa et al., 2021].

Of particular interest are the following cases:

1. 3HSP J095507.9+355101 is an extreme blazar, i.e., it belongs to the rare class of blazars whose low-energy component peaks beyond 1 keV. It is located at redshift  $z = 0.557$  and was detected in a high, very hard, and variable X-ray state shortly after the arrival of the high-energy neutrino IC 200107A [Giommi et al., 2020].
2. PKS 0735+17 is an IBL/HBL blazar at redshift  $z > 0.424$ , and a bright source in  $\gamma$ -rays  $> 100$  MeV. Based on its average  $\gamma$ -ray flux, it is ranked No. 19 among 1,500 IBL/HBL blazars included in the 4th *Fermi*-LAT catalog of AGN [Lott et al., 2020]. In December 2021, PKS 0735+178 was found to be in spatial coincidence with multiple neutrino events detected by the IceCube, Baikal, Baksan, and KM3NeT neutrino telescopes while undergoing its largest flare ever observed in the optical, UV, soft X-ray and  $\gamma$ -ray bands [see Sahakyan et al., 2022, and references therein].

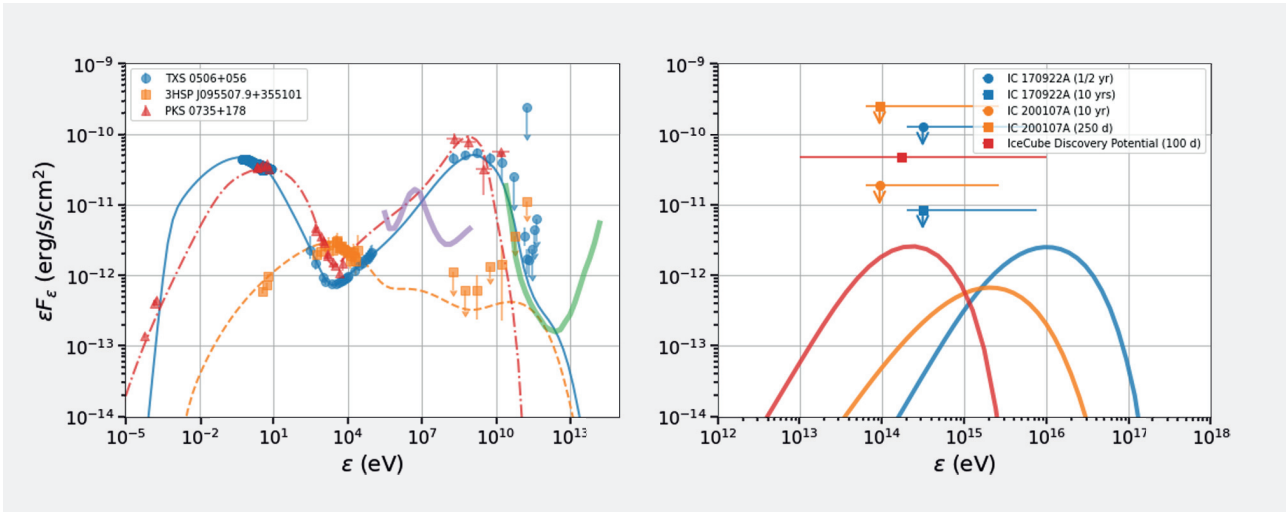
Model predictions about the neutrino fluxes vary considerably for blazars with different observational characteristics (e.g., spectral class and  $\gamma$ -ray luminosity). This is exemplified in Fig. 7 where we show SED models for the three flaring blazars TXS 0506+056, PKS 0735+178, and 3HSP J095507.9+355101, constructed using observations close to the time of arrival of IceCube neutrinos. Interestingly, both IBL blazars, TXS 0506+056 and PKS 0735+178, are well described by the hybrid model. Because of the great resemblance of their flaring SEDs, the peak neutrino fluxes are also very similar, and equal to  $\sim 10\%$  of their  $\gamma$ -ray fluxes. On the contrary, the HBL blazar 3HSP J095507.9+355101 can be modeled in the PC scenario where the neutrino flux is comparable to the  $\gamma$ -ray flux. Still, the neutrino flux of 3HSP J095507.9+355101 is lower than the other two sources, since HBL blazars are generally fainter in  $\gamma$ -rays than LBL and IBL blazars.

Fig. 8 summarizes the neutrino output and proton content of the three aforementioned blazar jets as inferred by SED modeling. For 3HSP J095507.9+355101 and PKS 0735+178 we show results from more than one models that describe well the SEDs, but have have different

parameter values. For TXS 0506+056 we show results from the same model when applied to archival observations besides the 2017 flare [Petropoulou et al., 2020]. There is an emerging trend that the neutrino-to- $\gamma$ -ray luminosity ratio,  $Y_{\nu\gamma}$ , decreases with increasing  $L_\gamma$ . In other words, the contribution of secondaries from photopion interactions to the high-energy blazar emission is smaller in sources that are more  $\gamma$ -ray luminous. The dependence of  $Y_{\nu\gamma}$  on  $L_\gamma$  is particularly important for models of the diffuse neutrino flux from the blazar population [Petropoulou et al., 2015]. IceCube upper limits from the non-detection of neutrinos at UHE constrain  $Y_{\nu\gamma} \leq 0.1$  [Aartsen et al., 2018].

Besides the actual neutrino flux, the predicted rate of muon neutrinos and anti-neutrinos,  $\dot{N}_{\nu_\mu+\bar{\nu}_\mu}$ , depends on the effective area of the detector and in turn on the source declination. In general, the yearly neutrino rates lie in the range 0.01–1 yr $^{-1}$ . When mapped to week-long flare durations, the model-predicted number of muon neutrinos is still much less than one. This may be regarded as unsatisfactory at first sight. However, the Poisson probability of observing one neutrino when the expectation is e.g., 0.1 is  $\sim 10\%$ , which is non-negligible and statistically consistent with the observations. We note that if the models predicted a number of  $\sim 1$  neutrino during flares, then, there would be a larger problem of consistency with other IceCube observational data.

The baryon loading factor,  $\xi$ , varies by many orders of magnitude, as shown in the middle panel of the figure. This highlights the strong dependence of  $\xi$  on the source parameters, such as radius and Doppler factor. Fits to UHE cosmic ray data allow  $\xi < 400$ , assuming that all UHE protons originate in blazar jets. This value is lower than what is required to account for the neutrino flux implied by the aforementioned blazar-neutrino associations. However, the values of  $\xi$  shown here cannot be constrained by UHE cosmic-ray observations, because the models do not predict proton acceleration to these energies. Moreover, all models displayed in the figure require super-Eddington jet luminosities, which is difficult to reconcile with theoretical models for jet launching [see discussions in Petropoulou et al., 2020].



**Figure 7:** Comparative plot of multi-messenger emission from three flaring blazars possibly associated with high-energy neutrinos. *Left panel:* Colored lines show model fits to the SEDs of blazars TXS 0506+056 (hybrid; blue), 3HSP J095507.9+355101 (hadronic PC; orange) and PKS 0735+178 (hybrid; red) close to the time of arrival of IC 170922A, and IC 200107A and IC 211208A, respectively. The planned 5 yr sensitivity of *AMEGO* (purple) [McEnery et al., 2019] and the 50 hr CTA North sensitivity (green) (adopted from Hinton & Ruiz-Velasco [2020]) are overplotted for comparison. *Right panel:* Model-predicted all-flavor neutrino energy fluxes for the three blazars. Same color coding used as in the left panel. Models and data are taken from Keivani et al. [2018]; Petropoulou et al. [2020]; Sahakyan et al. [2022]. Detailed references to the observations can be found therein.

## 5. Outlook

The experimental and theoretical findings we outlined in this contribution have already raised a number of important questions:

1. Is there a way to relax the energetic requirements of hadronic blazar models? Or a revision of our understanding of how jets are powered is needed?
2. Is there a particular subclass of blazars that is more promising for neutrino production? And if so, what are the physical reasons?
3. Are there any spectral features in the electromagnetic emission of blazars that one should search for when “hunting” for neutrino sources?
4. Are  $\gamma$ -ray photons and neutrinos always produced in the same part of the jet? Or, are there multiple locations for neutrino production in a blazar jet?
5. Are X-ray or UV photons perhaps a better probe of neutrino emission than  $\gamma$ -rays?

While we are still digesting the theoretical ramifications of the first likely neutrino-blazar association and what this means for the blazar population as a whole, we are faced with the challenge of a major boost in multi-messenger time-domain blazar observations within

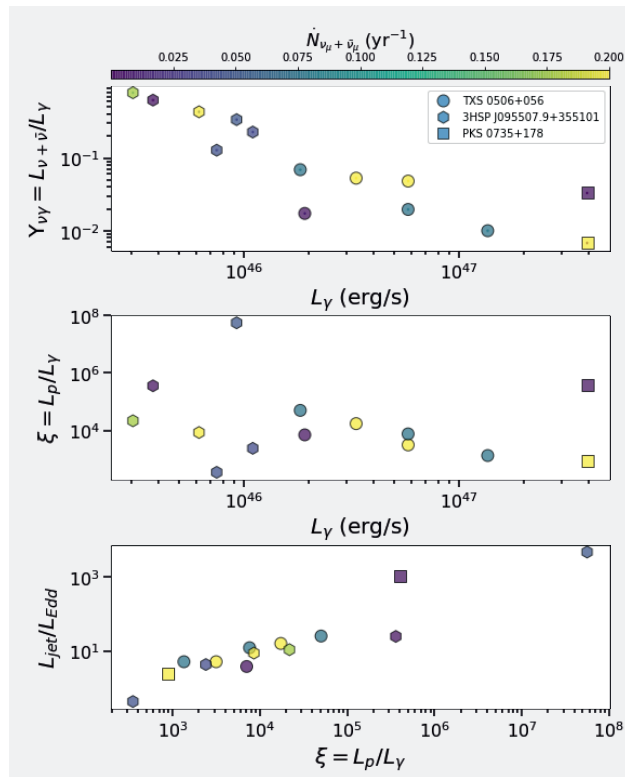


**Figure 8:** Comparative plot of inferred parameters from modeling of three flaring blazars possibly associated with high-energy neutrinos. *Top and middle panels:* The neutrino-to- $\gamma$  ray luminosity ratio  $Y_{\nu\gamma}$ , and the baryon loading factor  $\xi$ , as a function of the blazar  $\gamma$ -ray luminosity. *Bottom panel:* The jet luminosity normalized to the Eddington luminosity (assuming a black hole mass  $10^9 M_\odot$  loading factor.) as a function of the baryon loading factor.

the next decade [Santander et al., 2019]. This will be made possible by the construction of next-generation neutrino telescopes, i.e., IceCube-Gen2<sup>5</sup> [Aartsen et al., 2014], KM3Net<sup>6</sup> [Aiello et al., 2018], and P-ONE<sup>7</sup> [Agostini et al., 2020],

5. <https://icecube.wisc.edu/science/beyond/>
6. <https://www.km3net.org/>
7. <https://www.pacific-neutrino.org/>

combined with follow-up efforts and improvements in broadband coverage and sensitivity of new EM observatories, such as Large Synoptic Survey Telescope (LSST) [Robertson et al., 2017] in the optical, *STROBE-X* [Ray et al., 2019] in X-rays, and *AMEGO* in MeV  $\gamma$ -rays [McEnery et al., 2019]. Meanwhile, the Cherenkov Telescope Array (CTA) – planned to

be operational by the mid twenties – is expected to revolutionize our view of blazars at TeV energies thanks to its improved point-source sensitivity (about 10 times better than current Cherenkov telescopes) and superb energy and angular resolutions Acharya et al. [2018]. The research program “Unraveling the Non-Thermal Radiation PHysics Of Blazars (UNTRAPHOB)” (PI: M. Petropoulou), which was recently selected for funding by the Hellenic Foundation

for Research and Innovation, plans to address questions like those presented here. For this purpose, a comprehensive study of hadronic radiation models in the time-domain is proposed, augmented by simulations of spectra and light curves specifically designed for future instruments, like CTA. By developing a novel hadronic SED fitting tool, based on advanced statistical techniques to explore model parameter spaces, the inference of physical parameters for large

samples of blazars will become feasible. This will, in turn, provide a critical test for the applicability of hadronic radiation models to the general blazar population, and will allow a robust estimation of its contribution to the diffuse neutrino flux measured by IceCube. *In conclusion, the time is ripe to take stock of the current status, paving the path for an even brighter future in neutrino astrophysics.*



## References

- Aartsen, M. G., Ackermann, M., Adams, J., et al. 2018, *Phys. Rev. D*, 98, 062003
- Aartsen, M. G., Ackermann, M., Adams, J., et al. 2014, arXiv:1412.5106
- Aartsen, M. G. et al. 2013a, *Science*, 342, 1242856
- Aartsen, M. G. et al. 2013b, *Phys. Rev. Lett.*, 111, 021103
- Aartsen, M. G. et al. 2015, *Astrophys. J.*, 807, 46
- Aartsen, M. G. et al. 2017a, *Astrophys. J.*, 835, 151
- Aartsen, M. G. et al. 2017b, *Astrophys. J.*, 835, 45
- Aartsen, M. G. et al. 2018a, *Science*, 361, eaat1378
- Aartsen, M. G. et al. 2018b, *Science*, 361, 147
- Aartsen, M. G. et al. 2019, *Phys. Rev. Lett.*, 122, 051102
- Abdo, A. A., Ackermann, M., Agudo, I., et al. 2010, *ApJ*, 716, 30
- Acharya, B. S. et al. 2018, *Science with the Cherenkov Telescope Array*
- Agostini, M., Böhmer, M., Bosma, J., et al. 2020, *Nature Astronomy*, 4, 913
- Aiello, S. et al. 2018, arXiv:1810.08499
- Ajello, M., Gasparrini, D., Sánchez-Conde, M., et al. 2015, *ApJ*, 800, L27
- Albert, A. et al. 2018, *Astrophys. J.*, 868, L20
- Atoyan, A. & Dermer, C. D. 2001, *Phys. Rev. Lett.*, 87, 221102
- Bednarek, W. & Protheroe, R. J. 1999, *MNRAS*, 302, 373
- Blandford, R. D. & Payne, D. G. 1982, *MNRAS*, 199, 883
- Blandford, R. D. & Znajek, R. L. 1977, *MNRAS*, 179, 433
- Böttcher, M. 2019, *Galaxies*, 7, 20
- Böttcher, M., Reimer, A., Sweeney, K., & Prakash, A. 2013, *ApJ*, 768, 54
- Cerruti, M., Zech, A., Boisson, C., et al. 2019, *MNRAS*, 483, L12
- Dermer, C. D., Schlickeiser, R., & Mastichiadis, A. 1992, *A&A*, 256, L27
- Gao, S., Fedynitch, A., Winter, W., & Pohl, M. 2019, *Nature Astronomy*, 3, 88
- Garrappa, S., Buson, S., Francokowiak, A., et al. 2021, in *Proceedings of 37th International Cosmic Ray Conference — PoS(ICRC2021)*, Vol. 395, 956
- Garrappa, S. et al. 2019 [e-print[arXiv] 1901.10806] Giommi, P., Padovani, P., Oikonomou, F., et al. 2020, *A&A*, 640, L4
- Hartman, R. C., Bertsch, D. L., Bloom, S. D., et al. 1999, *ApJS*, 123, 79
- Hillas, A. M. 1984, *ARA&A*, 22, 425
- Hinton, J. & Ruiz-Velasco, E. 2020, in *Journal of Physics Conference Series*, Vol. 1468, *Journal of Physics Conference Series*, 012096
- Katrin Collaboration, Aker, M., Beglarian, A., et al. 2022, *Nature Physics*, 18, 160
- Keivani, A., Murase, K., Petropoulou, M., et al. 2018, *ApJ*, 864, 84
- Lott, B., Gasparrini, D., & Ciprini, S. 2020, arXiv e-prints, arXiv:2010.08406
- Mannheim, K. 1993, *A&A*, 269, 67
- Maraschi, L., Ghisellini, G., & Celotti, A. 1992, *ApJ*, 397, L5
- Mastichiadis, A. & Kirk, J. G. 1997, *A&A*, 320, 19
- McEnery, J., van der Horst, A., Dominguez, A., et al. 2019, in *Bulletin of the American Astronomical Society*, Vol. 51, 245
- Mücke, A. & Protheroe, R. J. 2001, *Astroparticle Physics*, 15, 121
- Murase, K., Inoue, Y., & Dermer, C. D. 2014, *Phys. Rev. D*, 90, 023007
- Murase, K., Oikonomou, F., & Petropoulou, M. 2018, *Astrophys. J.*, 865, 124
- Murase, K. & Stecker, F. W. 2022, arXiv e-prints, arXiv:2202.03381
- Padovani, P., Alexander, D. M., Assef, R. J., et al. 2017, *A&A Rev.*, 25, 2
- Padovani, P., Petropoulou, M., Giommi, P., & Resconi, E. 2015, *MNRAS*, 452, 1877
- Petropoulou, M., Dimitrakoudis, S., Padovani, P., Mastichiadis, A., & Resconi, E. 2015, *MNRAS*, 448, 2412
- Petropoulou, M., Oikonomou, F., Mastichiadis, A., et al. 2020, *ApJ*, 899, 113
- Rani, B., Petropoulou, M., Zhang, H., et al. 2019, *BAAS*, 51, 92
- Ray, P., Arzoumanian, Z., Ballantyne, D., et al. 2019, in *BAAS*, Vol. 51, 231
- Robertson, B. E., Banerji, M., Cooper, M. C., et al. 2017, arXiv:1708.01617
- Sahakyan, N., Giommi, P., Padovani, P., et al. 2022, arXiv e-prints, arXiv:2204.05060
- Sahu, S., Oliveros, A. F. O., & Sanabria, J. C. 2013, *Phys. Rev. D*, 87, 103015
- Santander, M., Buson, S., Fang, K., et al. 2019, *BAAS*, 51, 228
- Sikora, M., Begelman, M. C., & Rees, M. J. 1994, *ApJ*, 421, 153
- Swanenburg, B. N., Bennett, K., Bignami, G. F., et al. 1978, *Nature*, 275, 298

# The Extreme Environments of Luminous Infrared Galaxies

by Tanio Díaz-Santos

*Institute of Astrophysics, Foundation for Research and Technology-Hellas, Heraklion*

**G**alaxies are the beacons that enable us to study the structure of the Universe –from shortly after the Big Bang, up to the present day–, and pinpoint the location where gravity transforms mass into light, as gas collapses to form stars or as is being accreted into black holes (BH). Most galaxies, like our own –the Milky Way–, assemble their stellar mass in a steady manner, constituting what has been coined in the astrophysics community as the “main sequence” of star-forming galaxies, where more massive galaxies form stars at a progressively higher rates (Noeske et al. 2007; Elbaz et al. 2011). However, the most energetic phenomena in the Universe do not occur in these galaxies,

but within extreme systems triggered by galaxy mergers (see Fig. 1), that host nuclear, dust-enshrouded starbursts and/or ultra-luminous active galactic nuclei (AGN) powered by accretion onto supermassive black holes (SMBHs). Even though galaxies in this evolutionary phase do not dominate the integrated cosmic star formation or BH accretion rates of the Universe locally or at high redshift, they still account for a large fraction of both at any epoch (Schreiber et al. 2015). Moreover, this is a critical transition phase that will have a major impact on the history of the galaxies involved in the interacting process, likely prompting a dramatic morphological and physical transformation that will

convert the progenitors into a massive elliptical galaxy, suffering the irreversible quenching of star formation and BH growth due to feedback from the nuclear power source(s) (Hopkins et al. 2008). Therefore, extreme, luminous galaxies are one of the most fundamental pieces of the cosmic puzzle –a piece without which our understanding of the grand theory of galaxy formation and evolution would remain fundamentally incomplete.

## The beginning...

Pioneering work during the late 1960’s and the beginning of the 1970’s led to

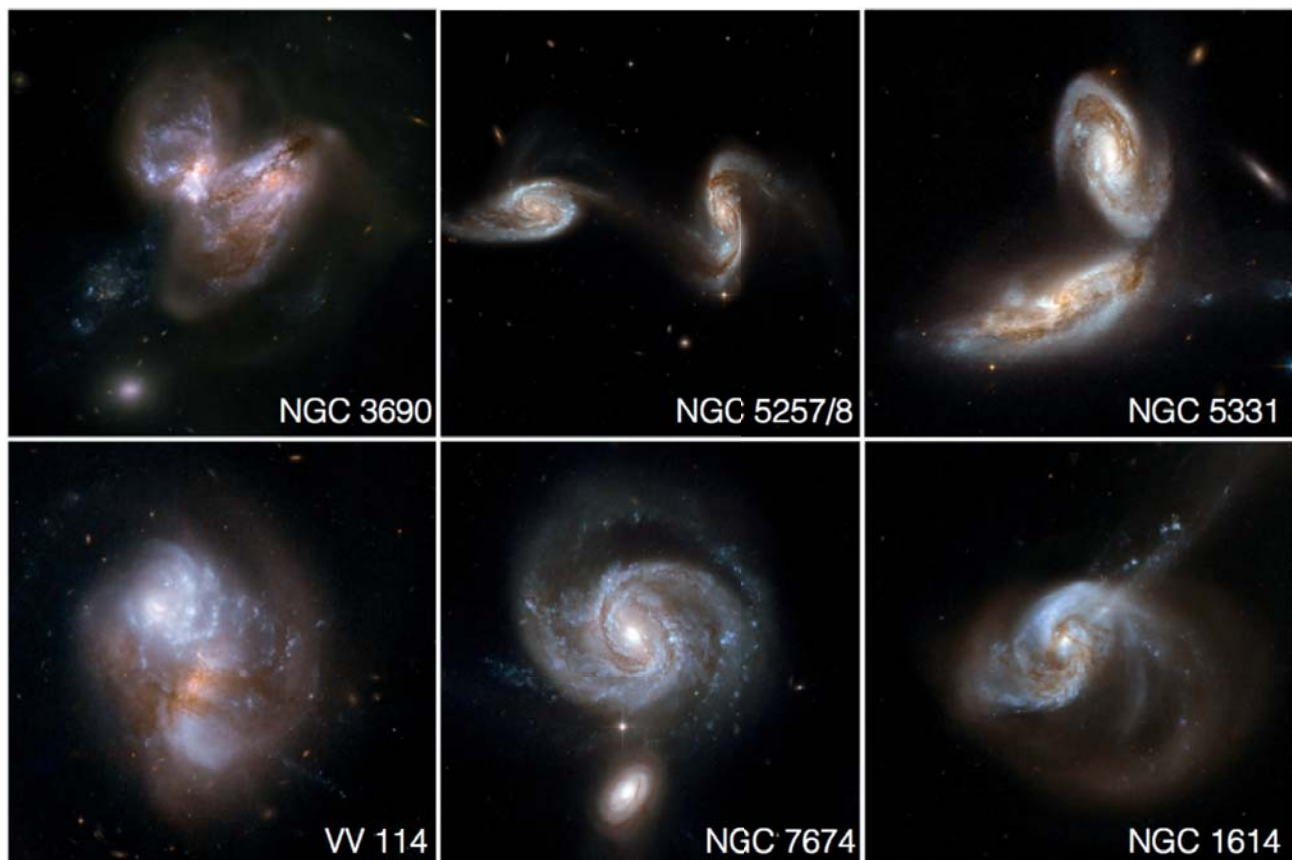


**Figure 1:** False-color images of six nearby luminous infrared galaxies, taken with the Hubble Space Telescope (HST). These images showcase the interacting nature of this galaxy population, the complex morphology and geometry of the dust obscuration they are subjected to, as well as their richness in star clusters and star-forming regions. Credit: Hubble Space Telescope.

the discovery that many galaxies that were bright at optical wavelengths, were even brighter in the infrared (IR) part of the spectrum, with luminosities that could reach  $10^{12}$  solar luminosities,  $L_{\odot}$  (Kleinmann & Low 1970; Rieke & Low 1972). All these galaxies, regardless of the internal processes that generate their IR luminosity, showed an increasing flux density towards longer wavelengths, radiating at their maximum in the mid- and far-IR (MIR, 5–25  $\mu\text{m}$ ; and FIR, 25–350 $\mu\text{m}$ , respectively). However, it took some years (until the late 1970's) for scientists to identify the physical process that leads to such prodigious power. It turned out that dust grains in the interstellar medium (ISM) of these galaxies absorb most of the internal ultraviolet (UV) and optical light generated by massive stars and AGN, and then re-emit it at IR wavelengths, with a spectral energy distribution similar to that of a black body at the temperature of the dust (Lebofsky & Rieke 1979; Telesco & Harper 1980).

This type of IR-bright objects immediately caught the interest of the scientific community, and the first ground-based MIR photometric studies of large samples of galaxies with strong star formation were carried out (Rieke & Lebofsky 1978; Lebofsky & Rieke 1979). These early works showed that the IR excess of those galaxies was actually a common property of extragalactic objects! Moreover, the IR continuum slope of many of these sources, with the exception of Seyfert galaxies and quasars, could be understood in terms of thermal emission of dust heated by star-forming processes. Note that nowadays it is generally accepted that the MIR and FIR emission of powerful Seyferts and most quasars is produced instead by dust irradiated by the accretion disk of their central SMBH. It was also at this time that the role of interactions in triggering the nuclear activity of IR-bright galaxies was identified (Larson & Tinsley 1978).

The decisive boost in our understanding of this galaxy population occurred with the launch of the IRAS space telescope (Neugebauer et al. 1984). Its sensitivity at 12, 25, 60 and 100  $\mu\text{m}$  allowed it to catalog new (and already detected) systems that emit the bulk of their luminosity in the MIR–FIR. In particular, luminous and ultra-luminous infrared galaxies, (U)LIRGs, were detected in the hundreds (see Sanders et al. 2003 for a

review). These systems show IR luminosities ( $L_{\text{IR}}$ ) larger than  $10^{11} L_{\odot}$  and  $10^{12} L_{\odot}$  respectively.

Subsequent studies (Soifer et al. 1987; Soifer et al. 1989) showed that, although (U)LIRGs are the dominant population in their luminosity range and are even more numerous (in density space) than optically detected quasars with same luminosities (Sanders et al. 1988a), they are not very common in the local Universe. However, the integrated IR luminosity of (U)LIRGs represent  $\sim 30\%$  of the total IR emission of the nearby Universe (Soifer & Neugebauer 1991). It was also unveiled that a large fraction of these galaxies are interacting systems (see, e.g., Borne et al. 2000; Bushouse et al. 2002). Moreover, the most luminous sources ( $L_{\text{IR}} \sim 3 \times 10^{12} L_{\odot}$ ) were classified as merger systems by default (Murphy et al. 1996). In addition, it was discovered that sources with high IR-to-UV ratios were mainly ( $\sim 70\%$ ) interacting systems, while the rest of galaxies were classified as amorphous or elliptical.

The detection of shocked molecular hydrogen,  $\text{H}_2$ , and other emission lines of (U)LIRGs in the near-IR (NIR) K-band suggested the presence of strong stellar super-winds, photoionized gas in HII regions, and high extinctions due to shocks caused by strong starbursts (Goldader et al. 1997). On the other hand, a significant fraction of nuclear optical spectra of (U)LIRGs showed emission lines typical of Seyfert galaxies. For instance, Veilleux et al. (1995) found that the fraction of galaxies with an AGN classification could be as high as  $\sim 50\text{--}60\%$  for systems with  $L_{\text{IR}} \geq 10^{12} L_{\odot}$ . Follow-up optical and NIR observations revealed that the probability of the presence of an AGN in the nucleus of a (U)LIRG increases with the IR luminosity of the system, and that the spatial distribution of the dust is more concentrated towards the circumnuclear regions. Other works also suggested that (U)LIRGs classified as Seyferts were more dynamically evolved systems than those dominated by star formation in which the dust would have already been destroyed or expelled from the nuclear regions due to powerful gas outflows. This was later on further supported by the fact that (U)LIRGs containing an AGN were more often found in evolved merger systems (Diaz Santos et al. 2010).

## New space telescopes, new discoveries

At the end of the 1990's, spectroscopic studies with the Infrared Space Observatory (ISO; Kessler et al. 1996) enabled the usage of numerous spectral lines produced by elements present in the ISM to trace diverse physical phenomena, such as HII regions photoionized by young, intense starbursts with large amounts of OB associations, photo-dissociation regions (PDRs; Hollenbach & Tielens 1997), shocks, regions of photoionized coronal gas, or gas excited by X-ray emission from a central AGN, without the limitations of the optical lines due to dust absorption (see Fig. 2). Diagnostic diagrams developed using spectral features detected in ISO spectra allowed the community to conduct detailed studies about the connection between the starburst processes and AGNs, and their contribution to the total luminosity of (U)LIRGs (Genzel et al. 1998).

ISO showed that the MIR (3–15  $\mu\text{m}$ ) spectra of starburst galaxies are dominated by a large number of emission bands (e.g., at 3.4, 6.7, 7.7, 8.6, 11.3, or 17  $\mu\text{m}$ ), known as polycyclic aromatic hydrocarbons (PAHs). Genzel et al. (1998) uncovered the existence of an anti-correlation between the maximum intensity of PAHs when compared to their continuum and the state of the ionized gas – a trend that could be explained by the presence of a heavily embedded AGN. Indeed, it was known from NIR spectroscopy that AGNs could be very obscured by dust (Goldader et al. 1997) –so extinguished that sometimes their true nature could only be uncovered in the MIR, where the dust is less opaque. However, such embedded AGNs do not seem to be very numerous, implying that the obscured-AGN phase should last for a short period of time, and once the AGN starts injecting feedback via galactic super-winds into the ISM, the hidden SMBH should become visible at short wavelengths (Lutz et al. 1999). Later studies determined that  $\sim 80\%$  of (U)LIRGs are dominated by starbursts, while the rest are explained by the presence of an active nucleus. Indeed, the fraction of LIRGs dominated by an AGN only increases significantly at luminosities higher than  $L_{\text{IR}} > 10^{12.3} L_{\odot}$ , when its contribution to the total luminosity output of the galaxy becomes  $> 50\%$ .

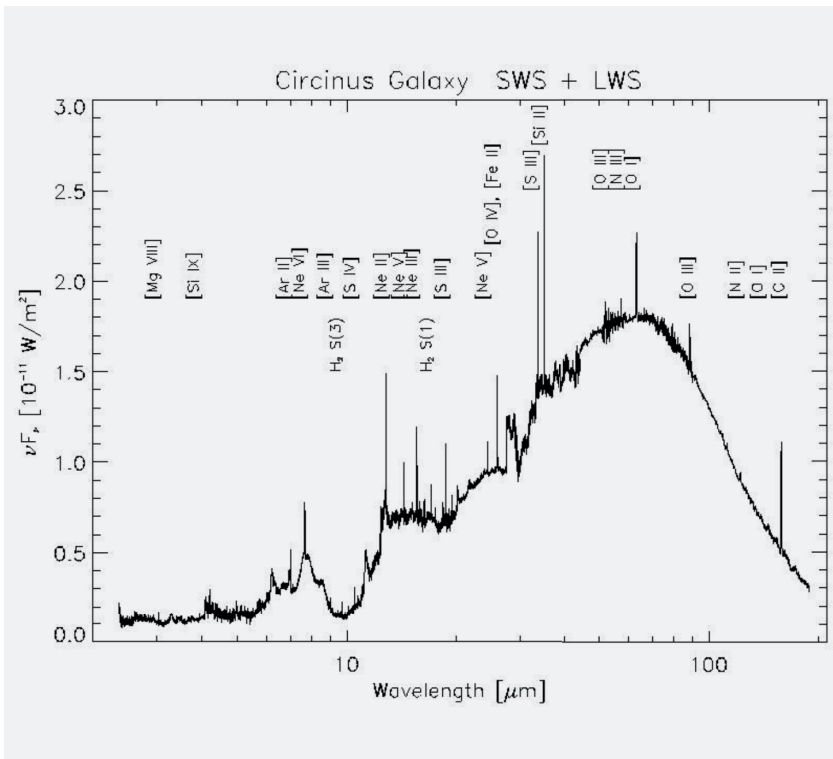


**Figure 2:** The IR spectrum of the Circinus galaxy taken with ISO. Many forbidden emission lines (labeled in between brackets) from fine-structure levels of a number of ions (Ar, Mg, Ne, S, O) can be seen in the spectrum. Highly ionized species result from gas heated by AGN, whereas emission from low ionization species originates from star forming activity. Taken from Moorwood (1997).

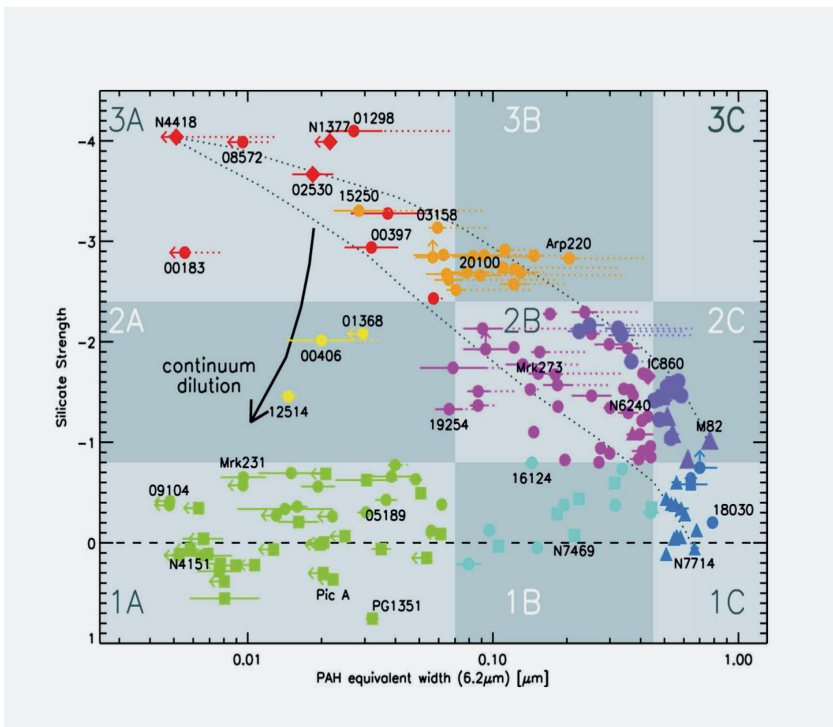


**Figure 3:** Diagnostic tool using the 6.2 μm PAH EW and the strength of the 9.7 μm silicate absorption feature for distinguishing between AGN and starburst-dominated sources. More negative values of the silicate strength means more obscuration. A lower PAH EW implies a larger contribution from the AGN to the MIR luminosity. As galaxies experience different phases in their evolution, they move through the different regions (shaded areas) on the diagram. Figure taken from Spoon et al. (2007).

## The IR revolution

And then... the Spitzer space telescope arrived in the early 2000's. The combination of the wavelength coverage, spectral and angular resolution, as well as its efficiency in collecting data with small overhead time offered by its Infrared Spectrograph (IRS; Houck et al. 2004), allowed us to obtain unprecedented high quality MIR spectra of large numbers of local LIRGs and ULIRGs. The spectra revealed an incredibly wide variety of features: high excitation forbidden emission lines, molecular hydrogen emission lines, PAH bands, absorption/emission features due to carbonaceous and silicate dust, among many other, which allowed for a truly detailed statistical interpretation of the physical processes taking place in these galaxies (Armus et al. 2007; Pereira-Santaella et al. 2010; Diaz-Santos et al. 2010, 2011; Stierwalt et al. 2013, 2014). Based on the slope of the MIR spectra, Spoon et al. (2007) used a diagram of the equivalent width (EW) of the 6.2 μm PAH versus the strength of the 9.7 μm silicate feature to distinguish galaxies dominated by star formation from galaxies dominated by an AGN. In this diagram the galaxies are placed in two branches, a horizontal one ranging from continuum-dominated (shallow silicate depth and low 6.2 μm PAH EW) to PAH-dominated (shallow silicate depth and large 6.2 μm PAH EW) spectra, and a diagonal one spanning between absorption-dominated (large silicate depth and low 6.2 μm PAH EW) and PAH-dominated spectra. Spoon et al. (2007) interpreted this bimodality in terms of two different geometries of the obscuring dust. Those sources presenting a deep silicate absorption feature would be deeply embedded and obscured by smoothly-distributed dust, while shallow silicate depths would be produced by clumpy distributions (see also Levenson et al. 2007).

During the late 2000's, similar spectral diagnostics like this helped to forge what is now considered the accepted paradigm of galaxy evolution within the merger-driven framework (Hopkins et al. 2008). During a major merger event between two massive, gas-rich spiral galaxies like our own Milky-Way (see Fig. 4), tidal torques and dynamical friction cause the molecular gas clouds to lose angular momentum. This cataclysmic event causes a large fraction of the interstellar gas and dust of the inter-

acting galaxies to be funneled toward their nuclei. The accumulation of gas on scales smaller than a kilo-parsec not only triggers massive bursts of star formation, but also feeds their central SMBH. However, this accretion of material occurs under the cover of darkness, hidden behind a thick veil of dust that has been piled up at the core of the galaxies (galaxies move in the diagonal branch of Fig. 3, from region 1C to region 3A). Once the starburst ignites and the central SMBH is activated, they are able to generate powerful feedback in the form of strong galactic winds and outflows that can expel out the remaining material that is still infalling, making the central AGN visible again (galaxies move from region 3A to 1A). This process is so violent that, in principle, it can potentially halt star formation in the host galaxy forever. During this period, galaxies move from region 1A to 1C, and then decay into elliptical galaxies.

### A step forwards (and outwards): The XTREME project

While there have been numerous works during the past decades dedicated to the study of the nuclear activity in nearby (U)LIRGs, only very few have investigated the properties of their extended disks and structures. As a consequence, the effect of the feedback from the nuclear power source (which is typically confined to the central kpc in the case of starbursts and/or to less than 100 pc in the case of AGN) on the surrounding ISM is largely unexplored –contrary to the extended ISM of normal star-forming galaxies, which has been extensively studied in the literature (e.g., Beirao et al. 2011; Smith et al. 2017). For LIRGs, the studies that have addressed this topic so far are limited in a number of ways: either the data do not allow for a complete control of the bias-

es (Diaz-Santos et. al 2010, 2011) and/or the analyses are constrained to describe particular observables at a specific wavelength, preventing the generalization of the results (Diaz-Santos et al. 2014).

Is the extended ISM of LIRGs in any way similar to that of their central core? Or does the nuclear activity affect its surroundings at large distances, beyond kpc scales? And if so, how and to what degree? Does the density or ionization state of the gas depend on the stage of interaction in merger systems? Do the properties of the extended star formation, such as the star formation efficiency, the specific star formation rate, or the gas depletion time-scale change as a function of distance to the LIRG nuclei? These are questions that have never been addressed so far in a comprehensive manner, and yet they are central to our understanding of the formation and evolution of one of the most important

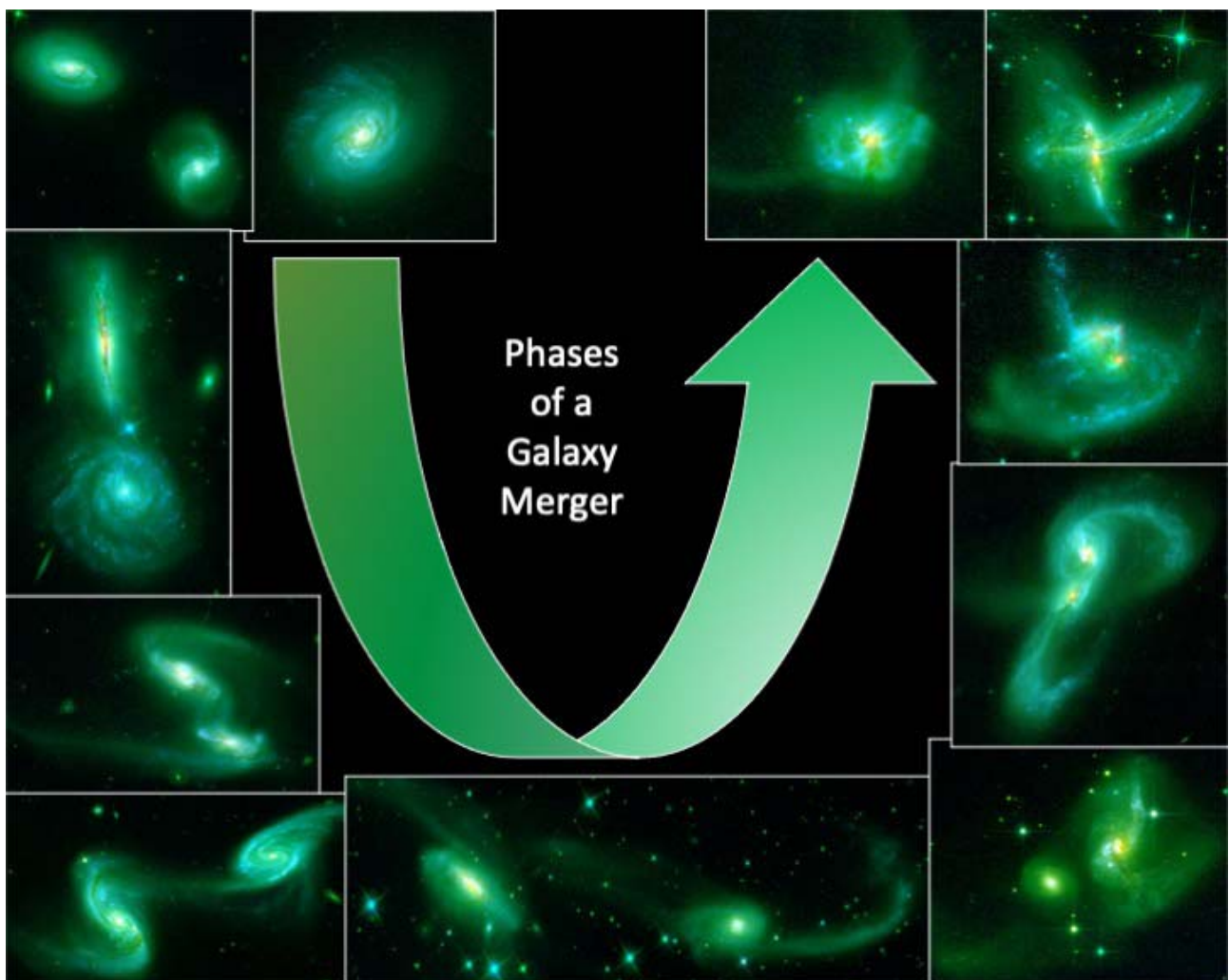


**Figure 4:** Schematic outline of the phases of growth in two “typical” disk galaxies undergoing a gas-rich major merger. All images are LIRGs from the Great Observatories All-sky LIRG Survey (GOALS; Armus et al. 2009), obtained with the HST.

population of galaxies in the Universe. The recently approved H.F.R.I. project entitled “The Extended Emission of Extreme Galaxies” (XTREME) aims to answer all these questions by performing a systematic multi-wavelength spectroscopic study of the physical properties of the extended regions of nearby LIRGs, combining the power of some of the largest ground- and space-based telescopes, past and present: the Spitzer Space Telescope, the Herschel Space Observatory, the Hubble Space Telescope (HST), and the Atacama Large sub-Millimeter Array (ALMA), the largest interferometric array of radio antennas ever built. These state-of-the-art facilities provide a broad coverage of the electromagnetic spectrum, from the UV/optical to the sub-millimeter, bringing into the table a large number of observables with which we can truly investigate the multi-phase nature of the ISM (see Tielens et al. 2005). A coherent picture of how the ionized, neutral and molecular gas phases in the extended regions of LIRGs are affected by the nuclear activity is only possible with a comprehensive, dedicated project like this, which makes use of all the multi-wavelength information at hand, and takes advantage of the synergistic nature of the greatest astronomical observatories.

## A connection between sub-kpc and kpc scales

### Kpc scales:

The spectral coverage provided by Spitzer, Herschel and ALMA observations, in combination with HST imaging data, provides an unprecedented cata-

log of fine-structure emission lines and dust spectral features that allows for a detailed characterization of the extended ISM in LIRGs at a resolution of a few kilo-parsec (kpc). XTREME’s multi-wavelength approach ensures that the line dataset is sensitive to a very large dynamic range in gas properties. Ionization potentials range from molecular and neutral atomic species, to highly ionized atomic lines such as [OIV]; and gas critical densities range from the diffuse molecular medium traced by the CO(J=2-1) line transition to the high densities probed by some neutral and molecular species. All emission lines are used simultaneously to derive the main parameters characterizing the ISM gas. This is achieved by using non-LTE radiative transfer models that simulate the physics of gas clouds with a variety of geometries, which are illuminated by the radiation of hot massive stars, the ambient interstellar radiation field, or an AGN. These theoretical models provide grids of emission line ratios parameterized based on the radiation field intensity and hardness of the ionizing source and the density and temperature of the exposed gas in its different phases (for example in PDRs; see Fig. 5), which can be directly compared with the data. The joint fit of all the ionized, atomic and molecular gas phases has been attempted before in a few bona-fide, individual star-forming regions, where such a wealth of data exists (Yeh et al. 2015). However, this is the first time where this methodology is applied systematically to a large sample of galaxies that range from normal isolated galaxies to starbursting/AGN dominated mergers.

### Sub-kpc, GMC scales:

XTREME also aims to investigate the properties of the extended ISM on the scale of individual giant molecular clouds (GMCs). The superb resolution of HST and ALMA enables the investigation of the physics of star formation down to  $\sim 100$  pc-size regions. The SFRs can be measured using optical and NIR hydrogen recombination lines with HST, while the molecular gas content is mapped in 3D by ALMA. This enables a direct comparison between the ongoing star formation and the availability of the gas reservoir to sustain it. In other words, when put together, these observations allow us to study how efficient star formation is, a critical property over which our understanding of galaxy evolution is built on. Using state-of-the-art searching algorithms for the identification of clusters in images and spectral cubes, we can characterize hundreds of star forming regions and gas clumps and study them not only as a function of the integrated properties of galaxies (stellar mass, merger stage, distance to the main-sequence, etc.) or their position within the galaxies (e.g., with galacto-centric distance to the nuclear power source), but also as a function of their environment. That is, we can investigate how the global conditions of the extended ionized and neutral ISM may influence the star formation and the molecular gas reservoirs on the smallest scales. This is the first time such a study is performed in LIRGs, allowing us to provide a statistically complete view on the formation and destruction of star clusters in galaxies along the complete merger sequence (Fig. 4), in and out of the MS of star-

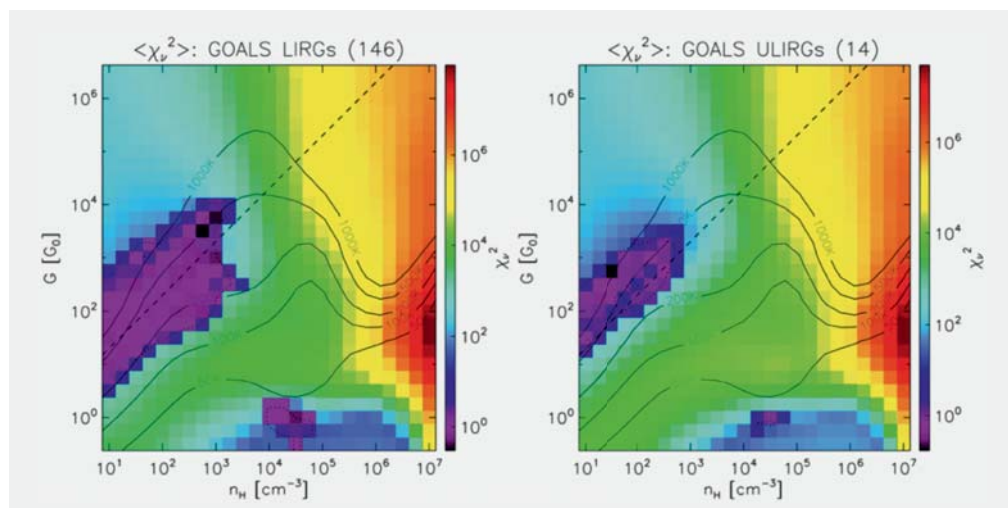


**Figure 5:** Example of results from a PDR modeling, using the PDR-Toolkit, of nearby LIRGs (left), and ULIRGs (right) (Diaz-Santos et al. 2017). The figures show the joint probability distribution for each sample,  $\langle \chi^2 \rangle$ , as a function of the interstellar radiation field  $G$  and the volume density of the gas,  $n_H$ . The best-fit values are the regions of the parameter space colored purple.

forming galaxies, and as a function of the local environment.

In summary, XTREME is a project that will investigate for the first time the physical properties of the extended star formation in LIRGs using a multi-wavelength, multi-scale approach based on spectroscopic data obtained by world-class telescope facilities. Using gas and dust tracers from the near to the sub-mm wavelengths, XTREME will study the extended multi-phase ISM, from kpc-size regions down to the scales of individual molecular gas clumps. And in doing so as a function of the integrated properties of galaxies and their merger stage, XTREME will serve as a reference benchmark with which to compare studies of clumpy star formation in systems that are currently being discovered by ALMA at a time when the Universe was much younger.

### A glimpse into the future: JWST

The James Webb Space Telescope (JWST) was launched on the 25th of December 2021 and it represents the flagship of the next-generation of IR telescopes. JWST aims to observe the early assembly of the first galaxies at an era when the Universe was less than one gigayear old –that is, less than 1/10th of the age it has today; down into the era of reionization ( $z > 6$ ). In the nearby Universe, JWST

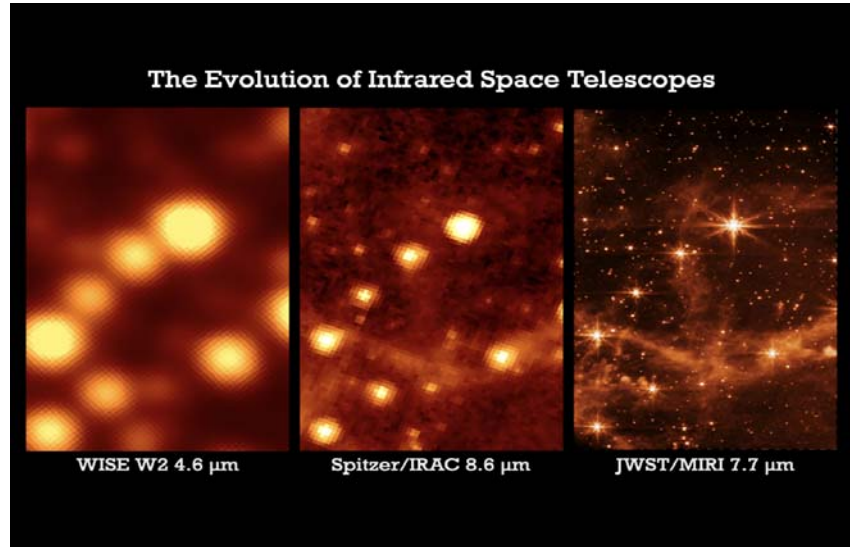


**Figure 6:** Comparison of spatial resolutions achieved with the WISE, Spitzer and JWST telescopes. Image credit: Andras Gaspar.

will provide an unprecedented view (see Fig. 6) on the physical processes that regulate star formation and SMBH accretion in the central kpc of LIRGs, as well as on the mechanisms that are able to launch the massive galactic outflows we observe at large scales. By the publication of this newsletter, JWST will have started to acquire the first imaging and spectroscopic data. In fact, some of the sources that the XTREME project is going to study will soon be observed as part of the Early Release Science program enti-

tled “A JWST Study of the Starburst-AGN Connection in Merging Luminous Infrared Galaxies” (P.I. Lee Armus; Caltech), as well as other Guaranteed Time Observations, in which the author of this paper is directly involved. The results produced by XTREME in the next coming years will therefore serve as a critical baseline with which to calibrate and put in context what JWST will find at the very core of this extraordinary class of extreme, luminous galaxies. ■

## References

- Armus, L., et al. 2015, *ApJ*, 656, 148  
 Beirão, P., et al. 2015, *MNRAS*, 451, 2640  
 Borne, K. D., et al. 2000, *ApJ Lett.*, 529, L77  
 Bushouse, H. A., et al. 2002, *ApJS*, 138, 1  
 Diaz-Santos, T., et al. 2010, *ApJ*, 711, 328  
 Diaz-Santos, T., et al. 2011, *ApJ*, 741, 32  
 Diaz-Santos, T., et al. 2014, *ApJL*, 788, 17  
 Diaz-Santos, T., et al. 2017, *ApJ*, 846, 32  
 Elbaz, D., et al. 2011, *A&A*, 533, 119  
 Genzel, R., et al. 1998, *ApJ*, 498, 579  
 Goldader, J. D., et al. 1997a, *ApJS*, 108, 449  
 Hopkins, P. F., et al. 2008, *ApJS*, 175, 356  
 Houck, J. R., et al. 2004, *ApJS*, 154, 18  
 Kessler, M. F., et al. 1996, *A&A*, 315, L27  
 Kleinmann, D. E., & Low, F. J. 1970, *ApJL*, 159, L165  
 Larson, R. B., & Tinsley, B. M. 1978, *ApJ*, 219, 46  
 Lebofsky, M. J., & Rieke, G. H. 1979, *ApJ*, 229, 111  
 Levenson, N. A., et al. 2007, *ApJ Lett.*, 654, L45  
 Lutz, D., Veilleux, S., & Genzel, R. 1999, *ApJL*, 517, L13  
 Moorwood A. F. M. 1999. See Cox & Kessler 1999, 825, 31  
 Murphy, Jr., T. W., et al. 1996, *AJ*, 111, 1025  
 Neugebauer, G., et al. 1984, *ApJL*, 278, L1  
 Noeske, K.G., et al. 2007, *ApJ*, 660, 43  
 Pereira-Santaella, M., et al. 2010, 2010, *ApJS*, 188, 447  
 Rieke, G. H., & Low, F. J. 1972, *ApJ Lett.*, 176, L95  
 Rieke, G. H., & Lebofsky, M. J. 1978, *ApJ Lett.*, 220, L37  
 Sanders, D. B., et al. 1988, *ApJL*, 328, L35  
 Sanders, D. B., et al. 2003, *AJ*, 126, 1607  
 Schreiber, C., et al. 2015, *A&A*, 575, 74  
 Smith et al. 2017, *ApJ*, 834, 5  
 Soifer, B. T., et al. 1987, *ApJ*, 320, 238  
 Soifer, B. T., et al. 1989, *AJ*, 98, 766  
 Soifer, B. T., & Neugebauer, G. 1991, *AJ*, 101, 354  
 Spoon, H. W. W., et al. 2007, *ApJL*, 654, L49  
 Stierwalt, S., 2014, *ApJ*, 790, 124  
 Telesco, C. M., & Harper, D. A. 1980, *ApJ*, 235, 392  
 Tielens, A.G.G.M., *The Physics and Chemistry of the Interstellar Medium*, 2005, Cambridge University Press.  
 Veilleux, S., et al. 1995, *ApJS*, 98, 171  
 Yeh, Sherry C. C., et al. 2015, *ApJ*, 807, 117

# Semi-empirical modelling of the Energetic Universe

by Antonis Georgakakis, Ivan Muñoz Rodríguez  
*National Observatory of Athens*

## 1. Introduction and Motivation

One of the most influential results in extragalactic astrophysics in the last two decades has been the realisation that all massive galaxy bulges in the local Universe host supermassive black holes of million to billion solar masses (Kormendy & Ho 2013). These compact objects are believed to grow their masses over cosmic time predominantly via accretion of material from their surroundings (e.g. Soltan 1982; Merloni & Heinz 2008). During these growth phases large amounts of energy are produced that can be detected as radiation at different parts of the electromagnetic spectrum. The class of astrophysical sources that correspond to such events are broadly dubbed Active Galactic Nuclei (AGN; Padovani et al. 2017). Understanding the physics of the accretion flow and the processes that trigger accretion events leading to the formation of supermassive black holes remain major challenges in current astrophysical research. Moreover, a physical description of the accretion history of the Universe has far reaching implications that go beyond the field of high energy astrophysics. It is believed that the growth of supermassive black holes is closely related to the evolution of the galaxies that host them (e.g. Brandt & Alexander 2015). Therefore understanding how AGN are triggered and how they affect their surroundings is a prerequisite for a complete picture of galaxy formation.

The main difficulty for developing a theory for the growth of supermassive black holes is that the relevant physical processes are complex, interconnected and operate on a broad range of spatial and temporal scales. They involve the lifecycle of gas (i.e. the main fuel of black holes) in galaxies, which in turn is linked to stellar evolution, the dynamics of galaxies and the large-scale cosmological environment in which they are embedded. An observationally motivated

approach to address this complexity and isolate the key physical conditions that promote accretion events onto supermassive black holes is to characterise the statistical properties of galaxies with active nuclei in relation to non-active ones. For example, observations of the structural parameters of AGN host galaxies in a cosmological volume informs on the role of galaxy interactions and secular processes (e.g. bars) in triggering AGN (Georgakakis et al. 2009, Cisternas et al. 2015). The position of active black holes on the cosmic web provides a handle on the influence of the environment in modulating the growth of black holes (e.g. Allevato et al. 2011, Fanidakis et al. 2013). Constraints on the stellar populations and star-formation histories of AGN hosts can be used to explore the interplay between stellar evolution and accretion events (Aird et al. 2019, Mountichas et al. 2022).

Observations on the population properties of AGN, like those outlined above, need to be complemented with models on the evolution of galaxies and their supermassive black holes to provide insights into the physics at play. The backbone of such models are cosmological theories of structure formation. In the current paradigm, the initial fluctuations in the density field of the dark-matter distribution in the Universe amplify with time and gravitationally collapse to form an evolving population of dark-matter haloes. These are the sites where baryonic matter can condense and form light-emitting structures, such as galaxies, that can be traced by their electromagnetic radiation. Fortunately, the evolutionary history of dark matter halos in a cosmological volume under the influence of gravity is well understood and can be modelled to a good level of accuracy using either analytic prescriptions (Press & Schechter, 1974, Bosch et al. 2014) or numerical N-body simulations (e.g. Klypin et al. 2016). The end product are merger trees that describe how dark matter halos grow

with cosmic time. The next challenge is to combine these merger trees with baryonic processes that describe galaxy evolution, such as gas cooling, the formation of stars, heating of the ISM via e.g. supernovae explosions or the energy produced by AGN, accretion flows onto black holes. Many of these processes are complex and cannot be modelled from first principles. As a result, physically motivated analytic prescriptions are adopted to parametrise them. These are then applied to the dark matter halo merger trees to simulate galaxy formation in a cosmological volume. The parameters of the various analytic prescriptions can then be tuned to reproduce Universes of galaxies and their supermassive black holes similar to the observed one. This approach leads to the broad class of Semi-Analytic Models (SAM), which have been extensively and successfully used to learn about the key physical mechanisms that drive galaxy evolution and trigger AGN (e.g. Somerville et al. 2008). One of the limitations of SAMs however, is the large number of tunable parameters and the aliases between them that affect their predictive power.

An alternative to SAMs are models that use empirical (i.e. observationally motivated or intuitive) relations to populate dark matter halo merger trees with galaxies and describe their properties, e.g. star-formation, morphology, black-hole mass or AGN luminosity etc. The power of this approach is that with a limited number of parameters and minimal physical assumptions it is possible to generate simulated Universes that closely mimic the real one. This class of models, dubbed Semi-Empirical (SEMs, Behroozi et al. 2013), are ideal for hypothesis testing, prediction making and more broadly forward modelling of populations in a cosmological volume. This is because by construction SEMs allow a firm handle on aliases between physical parameters and observational selection effects. A drawback of SEMs is

that their predictive power on physical processes is limited because they are built on statistical relations rather than physics. In that respect they should be regarded as complementary to SAMs. SEMs can reveal trends, which can then be tested in a physical context with SAMs.

In this article we demonstrate the power of SEMs by testing the relation between AGN and large scale (>1Mpc) environment. This is done by constructing mock observations (including selection effects, i.e. forward model) of AGN and galaxies in a cosmological volume under the zero order assumption that “the incidence of AGN in galaxies does not depend on their position on the cosmic web”. Comparison of the predictions of this forward model against observations on the clustering properties of AGN allows testing the zero order hypothesis. If discrepancies are found then the zero order assumption is rejected.

If not, then the hypothesis cannot be falsified, at least to the accuracy level of the observations. The motivation for this particular application are conflicting observational results in the literature on the role of environment in triggering accretion events onto supermassive black holes. Some studies argue for a link between AGN accretion modes and large scale environment (e.g. Alleinato et al. 2011; Fanidakis et al. 2013). Others suggest that the distribution of AGN on the cosmic web simply reflects the clustering properties of their host galaxies, i.e. no dependence on triggering mechanisms (Leauthaud et al. 2015, Mendez et al. 2016).

The next sections attempt to resolve this discrepancy using the semi-empirical approach. Section 2 discusses the technicalities of the model construction. Section 3 presents the comparison with the observations and demonstrates the flexibility of the SEMs to forward mod-

el AGN populations by accounting for observational uncertainties and selection biases. Our conclusions and future prospects are summarised in Section 3 of this article.

## 2. Constructing the AGN population model

The method we follow to construct a semi-empirical model of AGN and galaxies in a cosmological volume builds upon three recent key developments. The proliferation of large volume and high-resolution cosmological N-body simulations that describe the assembly of dark-matter haloes in the Universe (e.g. Riebe et al. 2013). The progress made in associating galaxies with dark-matter haloes (galaxy-halo connection), and state-of-the-art observational constraints on the incidence of AGN in galaxies (Galaxy-AGN connection). These steps are described in detail

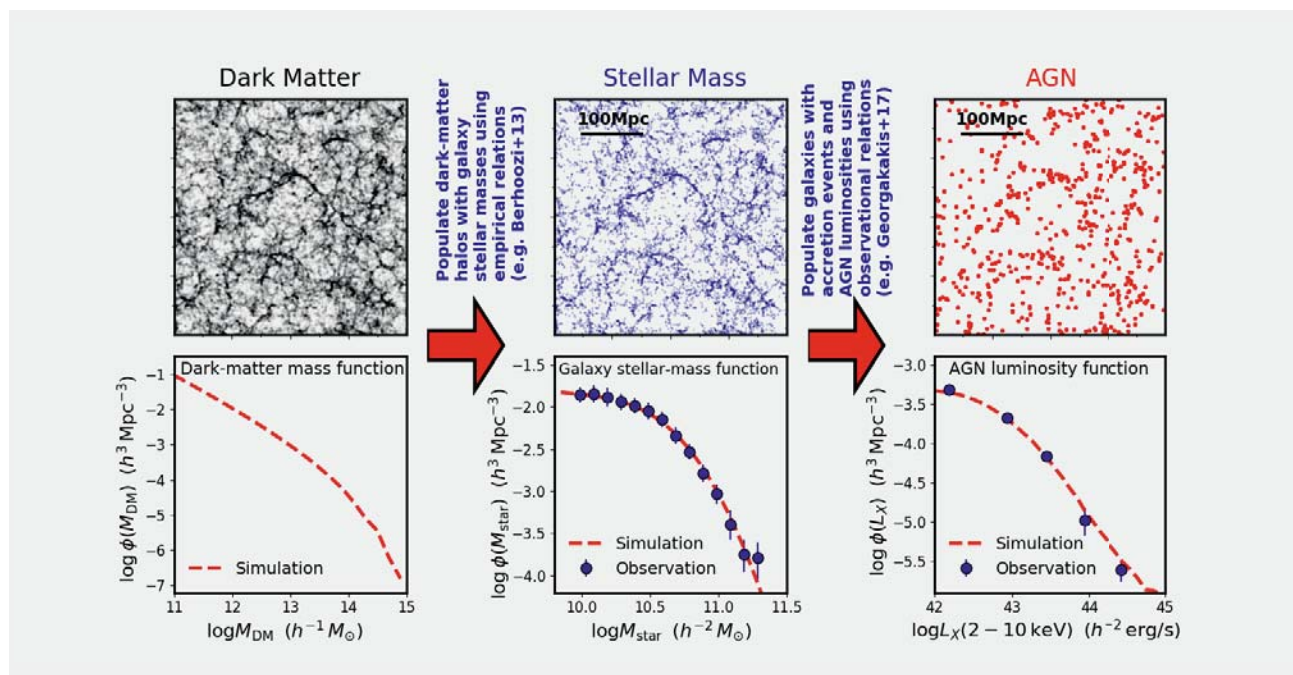


**Figure 1: Graphical representation of the semi-empirical AGN model construction:** The top set of panels are slices of a cosmological simulation box from the MultiDark project (Klypin et al. 2016) at a snapshot redshift  $z=0.75$ . It shows the positions of particles (e.g. left-top panel: dark matter halos; middle-top panel: galaxies; top-right panel: AGN) within the simulation box. Each particle in the simulation is represented by a dot (top-left panel: dark matter halos are shown with black; top-middle panel: galaxies are plotted in blue; top-right panel: AGN are shown in red). Darker regions mark a high density of particles, i.e. rich environments in the simulation. The filamentary structure of the matter distribution in the Universe, as a result of the gravity attraction, is clear in the distribution of particles shown in the top set of plots. The construction of the AGN semi-empirical model proceeds from left to right in this graphical representation: dark-matter halos (black dots in the top-left panel) in the simulation box are populated with galaxies (blue dots in the top-middle panel) using empirical relations between dark-matter halo mass and stellar mass (e.g. Behroozi et al. 2013). Accretion events are then distributed in these galaxies using observationally determined probabilities that a galaxy with a given stellar mass hosts an AGN with a given accretion luminosity (e.g. Georgakakis et al. 2017). In the top-right panel the mock AGN with accretion luminosity at X-ray wavelengths  $L_X > 10^{42} \text{ erg/s}$  are shown with red dots. The feature of this approach is that it starts from the simulated mass function of dark-matter halos in the Universe (red-dashed curve in bottom-left panel) and reproduces by construction the observed stellar mass function of galaxies (middle-bottom panel), and the luminosity function of AGN (right-bottom panel). The bottom-middle panel compares the galaxy mass function (space density of galaxies as a function of their stellar mass) in the semi-empirical simulation (red-dashed curve) and the real Universe (blue circles; Moustakas et al. 2013). The bottom-right panel plots the X-ray luminosity function of AGN (space density at fixed X-ray luminosity) in the semi-empirical simulation (red-dashed curve) in comparison with observational constraints (blue-circles) from Georgakakis et al. (2017).

below and are graphically demonstrated in Figure 1.

In a nutshell, the dark matter halos of the MultiDark PLanck2 (MDPL2, Klypin et al. 2016) cosmological N-body simulation are populated with galaxies using empirical relations (Behroozi et al. 2013) and then AGN are painted on these galaxies using observationally determined occupation probabilities (Georgakakis et al. 2017). The explicit assumption of the methodology is that the distribution of AGN in galaxies does not depend on the dark matter halo mass (or equivalently environment). Comparison of the model predictions with observations on the distribution of AGN on the cosmic web test this assumption.

### 2.1 Galaxy-halo connection: Abundance matching

The association of dark with luminous baryonic matter is based on the principle of abundance matching. The method relies on the idea that larger halos are associated with larger galaxies. In the simplest implementation halos and galaxies within a volume are ranked by their masses (dark and stellar respectively) and then objects of the same rank are paired. Despite its simplicity, this approach has proven successful in reproducing the observed distribution of galaxies on the cosmic web (Kravtsov et al. 2004; Vale & Ostriker 2004). A variation of this approach that is adopted here, assumes that each dark matter halo contains a single galaxy with stellar mass that is monotonically related to the halo mass of its host. N-body simulations provide information on the evolution and spatial distribution of dark-matter haloes within cosmological volumes. The abundance-matching method then populates these haloes with galaxy stellar masses by requiring that the statistical properties of the resulting mock galaxy population (e.g. stellar mass function, star formation properties, distribution on the cosmic web) match the plethora of observational data currently available (e.g. Behroozi et al. 2013).

For the analysis presented in this article the abundance matching model presented by Behroozi et al. (2013) is applied onto the halos of the MultiDark PLanck2 (MDPL2, Klypin et al. 2016) dark matter N-body simulation. The end product of this process are catalogues of mock galaxies and their associated dark matter halos. By construction these mocks are consistent with the ob-

served stellar mass function of galaxies in the Universe (see Fig. 1) as well as their clustering properties (i.e. distribution on the cosmic web).

### 2.2 AGN-galaxy connection: specific accretion rate distributions

The assignment of AGN to the mock galaxies generated by the abundance matching approach is based on empirical relations that link the probability of an accretion event onto a supermassive black hole to the properties of its host galaxy. The relevant observable is the specific accretion rate defined as the ratio of the accretion luminosity to the stellar mass of the galaxy that hosts the AGN,  $\lambda \propto L_{\text{AGN}}/M_{\text{star}}$ . Both quantities that enter the definition of the specific accretion rate can be inferred from observations:  $L_{\text{AGN}}$  can be approximated by the luminosity emitted by the accretion process at e.g. X-ray wavelengths, and  $M_{\text{star}}$  can be inferred by fitting templates to the multiwavelength spectral energy distribution of AGN host galaxies. In practice, the specific accretion rate provides an estimate of how much accretion luminosity is emitted by the AGN per unit stellar mass of the host galaxy.

Large multi-wavelength observational programs have enabled the estimation of stellar masses, X-ray luminosities and hence specific accretion rates for large AGN populations out to high redshift (Aird et al. 2012; Bongiorno et al. 2016; Georgakakis et al. 2017). These observations made possible the determination of the fraction of galaxies at fixed stellar mass that host an accretion event with specific accretion rate  $\lambda$ . These fractions can then be turned into specific accretion rate probability distri-

bution functions,  $P(\lambda)$ , that describe the probability of an accretion event with parameter  $\lambda$  in a galaxy. Examples of such probability functions are shown in Figure 2. The shape of the curve is intuitively sensible: high specific accretion rate events are rare among galaxies. This is demonstrated by the steep decrease of the curves toward high  $\lambda$  values. On the contrary, low specific accretion rate events are more common and the probability increases with decreasing  $\lambda$  and then flattens toward very low values. The shape of the curve in Fig. 2 is (nearly) equivalent to the observational fact that powerful QSOs (dominated by fast-accreting black holes) are sparse but low-luminosity Seyferts (mostly slow accreting black holes) are more common in the Universe.

The feature of  $P(\lambda)$  curves like the ones in Figure 2 is that they represent probability distribution functions. Put differently, given a sample of galaxies within a volume it is possible to use the  $P(\lambda)$  curves to probabilistically assign accretion events to them. This is the approach adopted for painting AGN onto the mock galaxies of the abundance matching approach. Each mock galaxy with stellar mass  $M_{\text{star}}$  is assigned a specific accretion rate,  $\lambda$ , that is drawn randomly from the observationally determined specific accretion-rate distributions. The end product of this process are catalogues of dark matter halos with associated mock galaxies of stellar mass  $M_{\text{star}}$  and AGN with specific accretion rate  $\lambda$  and hence, accretion luminosity,  $L_{\text{AGN}} \propto \lambda \cdot M_{\text{star}}$ . Figure 1 demonstrates that this semi-empirical methodology by construction reproduces the AGN luminosity function, i.e. the observed space

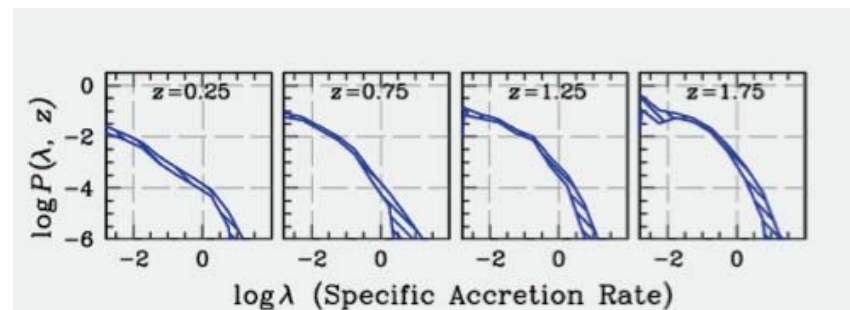


**Figure 2: Specific accretion-rate distribution:** the probability  $P(\lambda)$  of a galaxy hosting an accretion event of specific accretion rate  $\lambda \propto L_{\text{AGN}}/M_{\text{star}}$ , as a function of  $\lambda$ . The blue hatched regions are the non-parametric observational constraints on  $P(\lambda)$  presented in Georgakakis et al. (2017). The extent of the blue hatched regions provides an estimate of the observational uncertainty. Each panel corresponds to the specific accretion-rate distribution at different mean redshifts,  $z$ , indicated at the top of each panel.

density of accretion events in the Universe.

In the above process no distinction is made between galaxies at different environments (size of dark matter halo that hosts them). Therefore the SEM presented here assumes that the incidence of AGN in galaxies is independent of environment.

### 3. Comparison with observations

Next the predictions of the SEM are compared with observations of the distribution of AGN on the cosmic web. The approach taken in this comparison follows the principles of forward modelling. The simulations are engineered to resemble

real observations by applying to the model selection effects, such as the flux limits of real AGN/galaxy samples or the redshift intervals probed by different surveys. This step requires projecting the simulated catalogues of mock AGN and galaxies onto the sky plane and generating light cones like the ones shown in Figure 3. Such light cones resemble real extragalactic surveys, whereby individual objects are described by their sky coordinates (right ascension, declination) and radial distance to the observer (parameterized by redshift). It is on these light cones that observational biases that mimic those of real AGN and galaxy samples are applied.

These light cones are also used to estimate the same quantities that ob-

servers measure from real data to quantify how AGN/galaxies are distributed on the cosmic web. The statistic adopted in this article to describe this distribution is the (projected) two-point correlation function, which has been extensively used in the observational literature (Coil et al. 2009; Krumpe et al. 2012; Mountrichas et al. 2013). Briefly, this quantity measures how the distribution of extragalactic sources in the Universe differs from the random expectation. At a given physical separation it estimates the excess of AGN/galaxy or AGN/AGN pairs relative to those predicted from a random distribution of these sources. The (projected) two-point correlation function is therefore a measure of clustering strength at a given physi-

**Figure 3: Simulated light-cones that resemble real observations:** Pie-plot projection showing the distribution of mock galaxies (blue dots) and AGN (red circles) on the sky-redshift plane. The light cone is constructed by projecting a simulation box similar to that shown in Fig. 1 on the sky plane. The small blue symbols are galaxies tuned to follow the VIPERS survey selection function (Guzzo et al. 2014). The red circles are simulated AGN with a selection function that resembles that of the XMM-XXL survey (Liu et al. 2016).

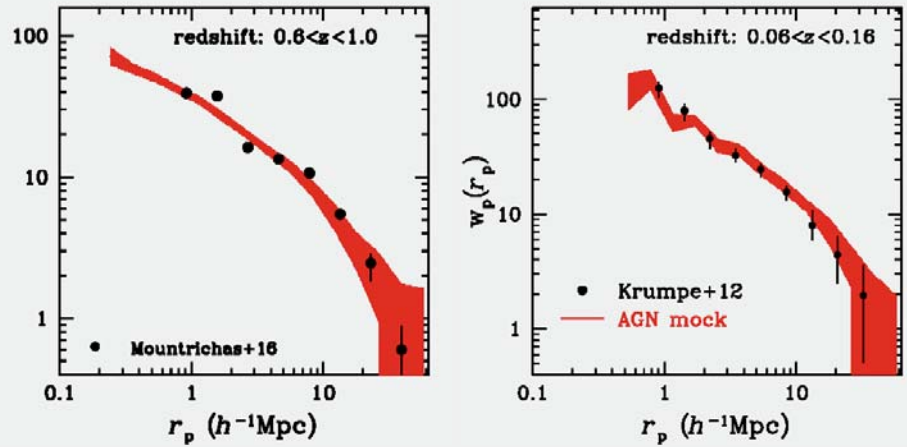
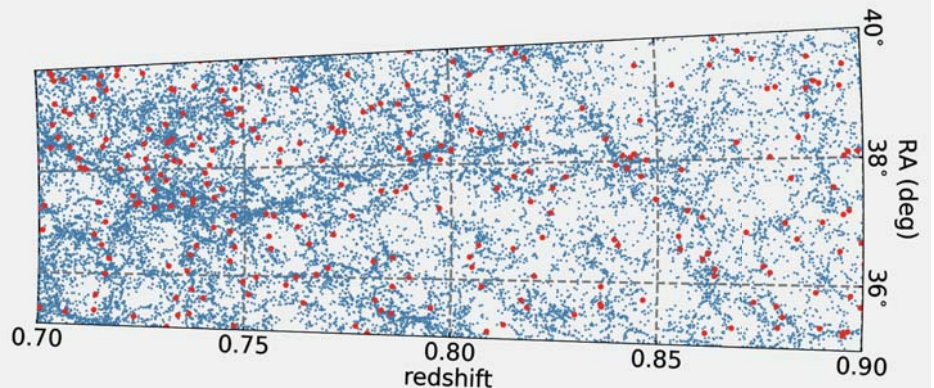


**Figure 4: Observations vs model predictions on the clustering of AGN:** The projected two-point correlation function of AGN samples. Each panel corresponds to a different observational study that selects AGN at different redshift and accretion luminosity intervals. The black data points in all panels correspond to the measured correlation function in Krumpe et al. (2012; left panel, redshifts  $0.06 < z < 0.16$ ), Mountrichas & Georgakakis (2012; middle panel, redshift  $0.02 < z < 0.2$ ) and Mountrichas et al. (2016; right panel,  $0.6 < z < 1.0$ ). The red curves are the correlation functions of the mock (simulated) AGN that follow the same selection criteria (redshift, accretion luminosity intervals) as the corresponding observational studies.



cal separation (or scale). The larger this statistic is, the more clustered the population is. A compilation of some of the most recent observational measurements of the (projected) two-point correlation function for AGN samples are shown in Figure 4. Each panel corresponds to a particular set of observations that probe AGN at different accretion luminosity and redshift intervals. Also overlaid in this figure are the predictions of the SEM described in this article. For each panel the SEM light cones are engineered to follow the observational selection effects of the corresponding sample (flux limits, luminosity/redshift intervals) and the (projected) two-point correlation function is measured in the same way as in the real observations.

A striking result from Fig. 4 is the remarkable consistency between observation and model predictions on the clustering AGN. The SEM under the zero order assumption that the incidence of AGN does not depend on environment or halo mass, can reproduce the observed clustering quite well. This

means that the zero order assumption cannot be rejected, at least within the error budget of the observational results shown in Figure 4. Put differently, the clustering of AGN is dictated by the properties of their host galaxies and does not point to a link between position on the cosmic web and AGN triggering mechanisms.

It should also be emphasised that the observations of Fig. 4 mostly measure the large-scale clustering of AGN i.e. on scales  $>1\text{Mpc}$ . On much smaller scales,  $<<1\text{Mpc}$ , which probe the immediate environment of individual galaxies/AGN, the observations plotted in Fig. 4 provide limited information. Our conclusion for the lack of a physical link between AGN triggering and position on the cosmic web therefore applies to the large-scale environment,  $>1\text{Mpc}$ . The methodology outlined in this article can be extended to also address the small-scale environment of AGN ( $<1\text{Mpc}$ ) and its relevance in promoting or suppressing accretion events onto supermassive black holes.

## 4. Concluding remarks

This article presents a methodology for constructing Semi-Empirical Models of AGN and galaxies in cosmological volumes and demonstrates their power for interpreting observational data on the statistical properties of active black holes. Large extragalactic surveys from e.g. the eROSITA telescopes at X-rays (Predehl et al. 2021) or in the near future the EUCLID mission in the optical/near-infrared (Laureijs et al. 2011) will significantly increase the volume and quality of observational data that can be used for population studies of AGN and galaxies. The interpretation of these observations also requires an effort at the modelling front. In this respect SEMs provide an important tool for understanding black-hole growth and galaxy evolution by allowing hypothesis testing and the forward modelling of observations.



## References

- Aird J. et al., 2019, *MNRAS*, **484**, 4360  
Aird J. et al., 2012, *ApJ*, **746**, 90  
Allevato V. et al., 2011, *ApJ*, **736**, 99  
Behroozi P. S., et al., 2013, *ApJ*, **770**, 57  
Bongiorno A. et al., 2016, *A&A*, **588**, A7  
Bosch F. C. v. d., Jiang F., Hearin A., Campbell D., Watson D., Padmanabhan N., 2014, *MNRAS*, **445**, 1  
Brandt W. N., Alexander D. M., 2015, *A&ARv*, **23**, 1  
Cisternas M., Sheth K., Salvato M., Knapen J. H., Civano F., Santini P., 2015, *ApJ*, **802**, 137  
Coil A. L. et al., 2009, *ApJ*, **701**, 1484  
Fanidakis N. et al., 2013, *MNRAS*, **435**, 679  
Georgakakis A. et al., 2009, *MNRAS*, **397**, 623  
Georgakakis A., Aird J., Schulze A., Dwelly T., Salvato M., Nandra K., Merloni A., Schneider D. P., 2017, *MNRAS*, **471**, 1976  
Guzzo L. et al., 2014, *A&A*, **566**, A108  
Klypin A., Yepes G., Gottlöber S., Prada F., Heß S., 2016, *MNRAS*, **457**, 4340  
Kormendy J., Ho L. C., 2013, *ARA&A*, **51**, 511  
Krautsov A. V., Berlind A. A., Wechsler R. H., Klypin A. A., Gottlöber S., Allgood B., Primack J. R., 2004, *AJ*, **609**, 35  
Krumpe M., Miyaji T., Coil A. L., Aceves H., 2012, *ApJ*, **746**, 1  
Laureijs, R., Amiaux, J., Arduini, S., et al. 2011, *arXiv*, e-prints, arXiv:1110.3193  
Leauthaud A. et al., 2015, *MNRAS*, **446**, 1874  
Liu Z. et al., 2016, *MNRAS*, **459**, 1602  
Mendez A. J. et al., 2016, *ApJ*, **821**, 55  
Merloni A., Heinz S., 2008, *MNRAS*, **388**, 1011  
Mountrichas G., Georgakakis A., 2012, *MNRAS*, **420**, 514  
Mountrichas G. et al., 2013, *MNRAS*, **430**, 661  
Mountrichas G., Georgakakis A., Menzel M.-L., Fanidakis N., Merloni A., Liu Z., Salvato M., Nandra K., 2016, *MNRAS*, **457**, 4195  
Mountrichas G., et al., 2022, *A&A* in press, arXiv:220501451  
Moustakas J. et al., 2013, *ApJ*, **767**, 50  
Padovani P., et al., 2017, *A&ARv*, **25**, 2  
Predehl P., et al., 2021, *A&A*, **647A**, 1  
Press W. H., Schechter P., 1974, *AJ*, **187**, 425  
Riebe K. et al., 2013, *Astron. Nachr.*, **334**, 691  
Soltan A., 1982, *MNRAS*, **200**, 115  
Somerville R. S., et al., 2008, *MNRAS*, **391**, 481  
Vale A., Ostriker J. P., 2004, *MNRAS*, **353**, 189

# Revisiting star and planet formation in the era of Big Data

by Odysseas Dionatos

Department of Astrophysics, University of Vienna, Austria



**Figure 1:** Ejection of material from a young stellar embryo (HH111). HST/Bo Reipurth.

## 1. Introduction

It is only 27 years since Mayor & Queloz (1995, Nobel Prize in 2019) reported the first discovery of an extrasolar planet around a sun-like star, initiating what has become one of the most rapidly developing areas in astrophysics and space research.

Today, more than 5000 exoplanets have been identified, a number that continues increasing. Understanding however the architecture of planetary systems, the composition of planets, and in this context the formation of the solar system, is not possible without addressing the bigger picture of star formation that precedes and accompanies the formation and early evolution of planets. Stars form as the end products of instabilities within dense molecular clouds, leading to a gravitational collapse of cloud cores to protostars. The main processes observed today to engage in the making of stars are the same processes responsible for the formation of the first solids in our solar system (e.g. chondrules and calcium-aluminium-rich inclusions). Therefore an accurate description of the processes, phases and timescales relevant to the creation of stars and planets are important not only for star-formation studies *per se*, but are also essential for understanding the formation of our own solar system and setting the prerequisites for habitability on exoplanets.

The formation of stars and planets has become one of the central areas of research in astrophysics showing a rapid development since the mid 1980's, boosted to an unprecedented level by the continuous development of space-borne infrared missions and ground-based millimeter submillimeter facilities. Classification schemes describing the evolution of Young Stellar Objects (YSO) introduced therefore more than 30 years ago, rely solely on a limited set of dust properties of the surrounding disk and envelope cannot provide an accurate description of the multitude of processes that regulate the formation timescales. In following sections I am reviewing the standard scheme describing the evolution of YSO, discuss the main theoretical and observational evidence questioning this formation scenario

and conclude providing an overview of the major developments that are currently transforming the field.

## 2. Star formation in a nutshell

Protostellar formation and growth occurs due to mass accumulation onto a central source through the mediation of an accretion disk. At the same time, the mass accretion is always followed by ejection of material forming collimated jets (Fig. 1) and wide-angle outflows. Being obscured behind their thick natal envelope, protostars remain quite intricate in their observational identification. The first efforts for a systematic classification of the different phases of star-formation became possible only in the 1980's, as a result of the first infrared surveys (IRAS<sup>1</sup>) combined with theoretical studies on the collapse of dense, rotating cores (Lada 1987; Shu et al. 1987).

Based on the shape of the Spectral Energy Distribution (SED), and in particular of the slope between  $2\mu\text{m}$  and  $20\mu\text{m}$  of forming stars, Lada (1987) defined three main phases to describe the complete evolution from an initial core-collapse to a pre-main sequence star: (i) the protostellar phase in which the central object is still embedded in its parental envelope; (ii) the pre-main sequence disk phase, where the envelope is dispersed and the circumstellar disk can be directly observed (accreting T-Tauri stars belong to this phase) and (iii) the pre-main sequence phase where the star's gas disk has essentially been dispersed. These three phases were coined as Classes I, II and III, and remain until today the main classification criterion used to study the formation of YSOs. The so-called Class 0 phase was only introduced in the 1990's when a new type of very young protostars that has acquired less than 50% of their envelope material was first detected (see Fig. 2, Andre et al. 1993). Shortly after, another "Flat-spectrum" group was added to describe sources possibly in transition between the Class I and the Class II phases (Greene et al. 1994). As an alternative classification criterion the bolometric temperature,

1. The Infrared Astronomical Satellite (IRAS, 1983), was the first infrared space telescope to perform a complete sky survey.

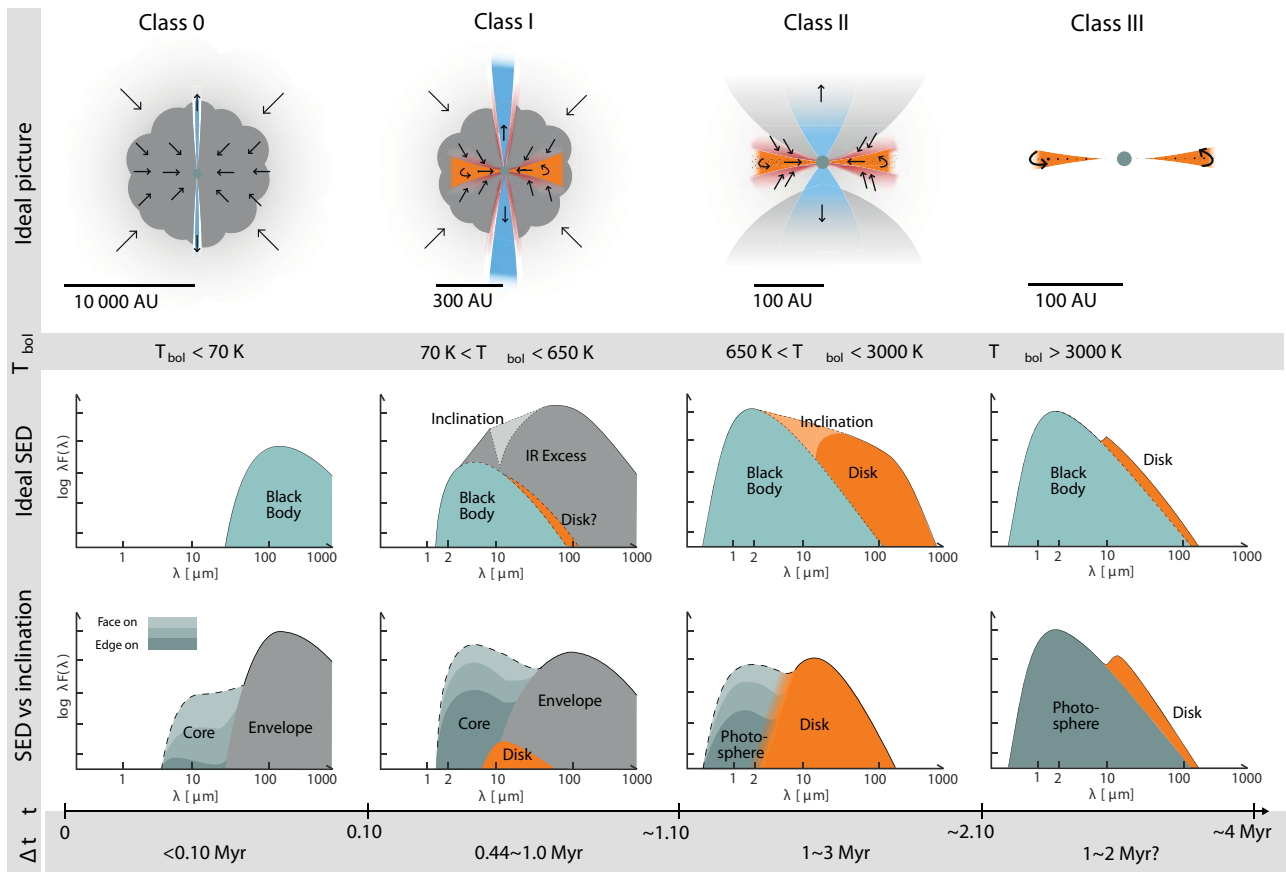


**Figure 2:** Schematic drawing of some of the important stages involved in the formation of low mass protostars (top row) along with their corresponding idealized SED's (middle row) and estimated SEDs at different inclinations. Phases follow the classification scheme defined by Lada (1987) further complemented with the Class 0 phase by Andre et al. (1993), and timescales are taken from Evans et al. (2009). As demonstrated in the lower panel, inclination renders a pure SED-based classification challenging and many in cases erroneous, as the SED morphology becomes degenerate between classes.

defined as the temperature of a black-body whose spectrum has the same mean frequency as the source (Ladd et al. 1991) was subsequently introduced (Myers & Ladd 1993). The notion that diagrams of bolometric temperature versus bolometric luminosity (in log-log space) are closely related to the H-R diagrams meant that an increase in bolometric temperature could better describe the evolution of young stellar objects as a process of consumption of the cold, protostellar envelope (and subsequently disk), revealing an increasingly hotter central object.

### Formation timescales

According to the standard classification paradigm (Lada 1987; Andre et al. 1993) as propagated and completed in a rapidly growing field (Stahler & Palla 2004), the formation of stars is a smooth process; central sources accumulate mass faster when they are younger (Class 0/I

phases), with estimated accretion rates dropping by an order of magnitude when crossing from one Class to another (from  $\sim 10^{-5} - 10^{-4} M_{\odot} \text{yr}^{-1}$  in Class 0 to  $\sim 10^{-9} - 10^{-8} M_{\odot} \text{yr}^{-1}$  in Class II/III). Conversely, a protostar spends increasingly more time in each phase, roughly by an order of magnitude. Inferred formation timescales (see Fig. 2) are also in accordance with surveys of the relative populations of sources belonging to different classes, as observed in nearby star-forming regions - under the assumption that such environments contain protostars formed at a single event. Toward the end of the star-formation process, pre-mainsequence sources can be placed on an H-R diagram and therefore their ages can be estimated with the use of models; these ages then provide the reference point for a backward extrapolation, based on simple number statistics on the occurrence of sources at different Classes, to estimate the du-

ration for each individual phase. Under these assumptions, median lifetimes for the Class 0, I, and II YSO correspond to 0.16 Myr, 0.54 Myr, and 2.0 Myr (Evans et al. 2009).

According to the standard formation scenario, planet formation occurs rather late, starting during the Class II phase with the material remaining in the accretion disk. The planet formation process presumably lasts for tens of Myr as the result of numerous constructive and destructive collisions between dust aggregates forming over time gradually larger structures. This is inline with comparison of the ages of planets and minor bodies in our solar system to the star-formation timescales directly suggests planet formation occurs quite late and when the formation of the star is almost complete (during the Class II and III phases for gaseous giants and rocky planets, respectively; Apai & Lauretta 2010).

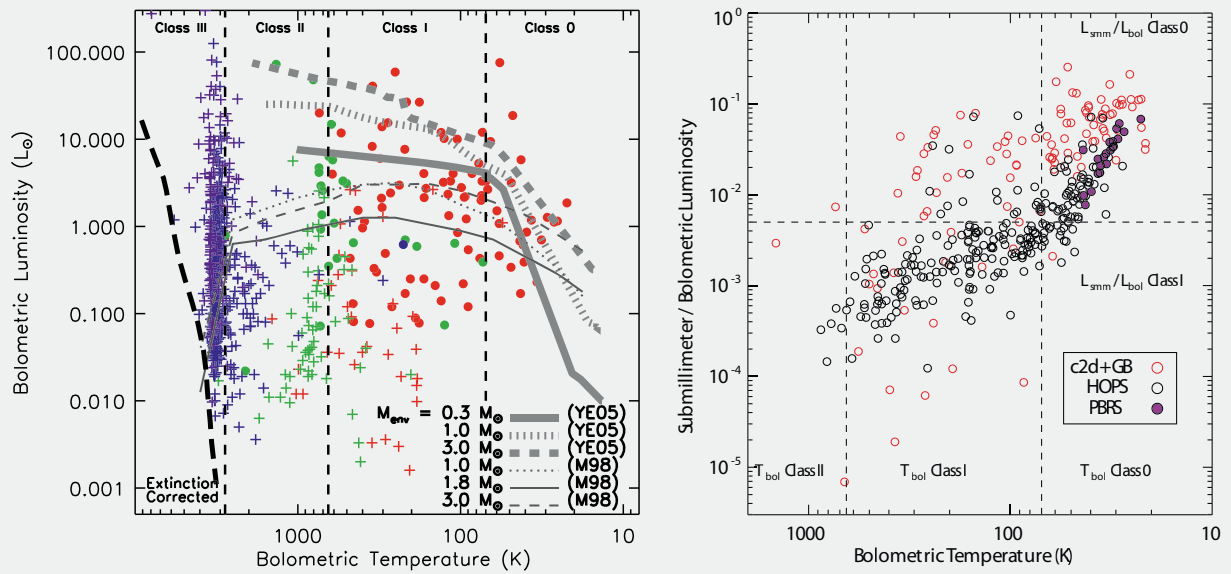


**Figure 3:** Comparison of SED-based evolutionary indicators for protostars: Bolometric temperature against the bolometric luminosity along with different theoretical evolutionary tracks (Evans et al. 2009, left) and against the submillimeter to bolometric luminosity ratio (Dunham et al. 2014, right). The submillimeter to bolometric luminosity ratio can better distinguish between different evolutionary classes of protostars, however scattering of data points remains very high and no clear boundaries exists. This is potentially one source for the scatter when only classifying with  $T_{bol}$  and  $L_{bol}$ .

### Cosmochemistry and the formation of the solar system

Coordinated efforts have been undertaken during the last decade, aiming in consolidating our understanding for the formation of the Sun and the Solar System in the context of star-formation. These efforts to a major part are concentrated in connecting the formation of the first solids in our solar system with the dust processing currently occurring around forming stars. Analysis of the isotopic composition of meteoritic materials are used to determine ages of CAI and chondrules. Certain families of chondrules and Calcium Aluminum Rich inclusions (CAIs) represent the oldest dust aggregates in the solar system. Assuming their ages coincide with the earliest stages of star formation (i.e. Class 0 phase), then we can correspond when the formation of different classes of solids were created in the context of star-formation (Connelly et al. 2012). Still, the formation route of chondrules is debated, where suggestions include planetesimal collisions (e.g. Wakita et al. 2017) which would then corroborate the idea from star formation studies of an early formation of planets (see below). From a different perspective, processes leading to fractionation of different

isotopologues of molecules have been also employed to anchor the formation of our solar system to the gas processes around protostars. The chemical evolution of water, for example, within the star formation process can have a direct impact to the initial conditions of planet formation. The water deuterium fractionation ( $\text{HDO}/\text{H}_2\text{O}$  abundance ratio) has traditionally been used to infer the amount of water brought to Earth by comets. Measuring this ratio in deeply-embedded low-mass protostars makes it possible to probe the critical stage when water is transported from clouds to disks in which icy bodies are formed.

### Revisiting the standard formation scenario

**Geometry:** An increasing number of studies during the last decade question the integrity of the standard star and planet formation paradigm. Formation timescales are mainly derived from population studies, which largely depend on the accuracy of the assumed classification criteria. In turn, Classes for young stellar objects are defined solely on particular characteristics of their SED which cannot effi-

ciently differentiate between different evolutionary stages, so they are prone to large uncertainties due to effects of inclination, aspherical geometries and reddening (e.g. Enoch et al. 2009; Dunham et al. 2014). The current classification criteria fail to provide a convincing representation for the evolution of YSO (see for example  $T_{bol}$  in Fig. 3). To this end Stages, which describe the true evolutionary phase of YSO unaffected by observational biases have been proposed to tackle observational biases (e.g., Dunham et al. 2014). Removing observational biases and therefore deriving Stages from the Classes of individual objects is not straightforward as it requires knowledge of the detailed 3D geometry of the dust component surrounding YSOs, including information on the shape, density structure, size of outflow cavities of flaring - when it comes to disks.

### Accretion and Ejection

Beyond classification, indirect methods for assessing formation lifetimes are based on estimates of the mass accretion rates. In the case such rates are derived from the mass flux of protostellar ejecta, a 10% ejection to accretion ratio is usually assumed that is derived

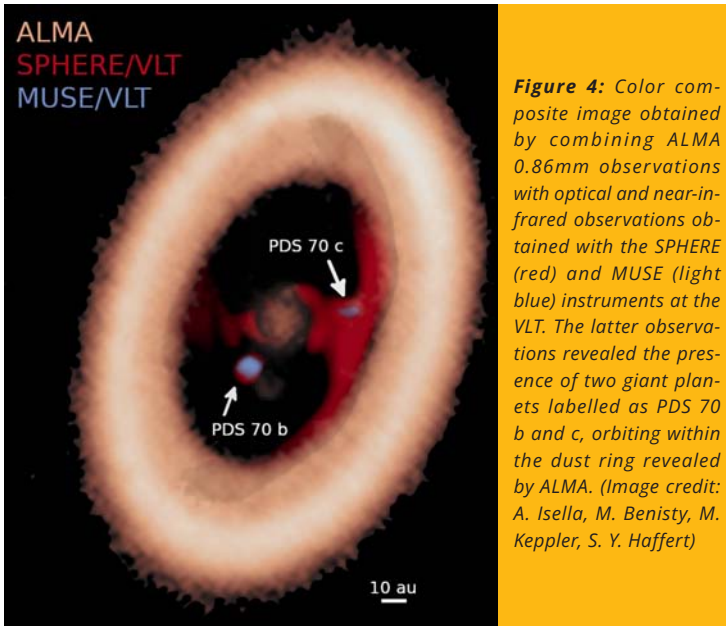


**Figure 4:** Color composite image obtained by combining ALMA 0.86mm observations with optical and near-infrared observations obtained with the SPHERE (red) and MUSE (light blue) instruments at the VLT. The latter observations revealed the presence of two giant planets labelled as PDS 70 b and c, orbiting within the dust ring revealed by ALMA. (Image credit: A. Isella, M. Benisty, M. Keppler, S. Y. Haffert)

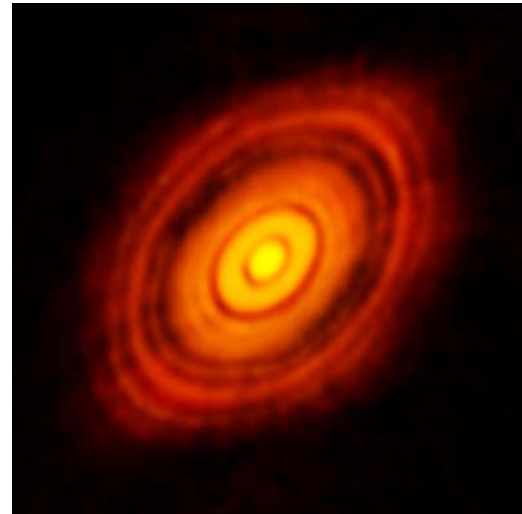


**Figure 5:** The HL Tau disk image at 1mm, obtained as part of the ALMA large baseline campaign (ALMA Partnership et al. 2015)

mainly from studies of T Tauri stars but is assumed to be valid for all phases of star formation. This ratio can, however, be very different in the case of younger sources and, therefore, the inferred accretion rates are uncertain.

When accretion rates are derived from the bolometric luminosity, then either mass accretion appears to be too slow or protostars appear to be underluminous (e.g. Kenyon & Hartmann 1990; Dunham et al. 2014). Mass accretion rates can also be derived using a combination of accretion-driven emission lines from the UV to the infrared (e.g. Rigliaco et al. 2012, 2015; Manara et al. 2016). Still, the two proxies for inferring mass accretion, i.e. the bolometric luminosities and the mass flux of outflows tightly correlate, indicating a physical connection between the two phenomena (e.g. Bontemps et al. 1996; Dionatos et al. 2010). Episodic accretion events can explain the low-luminosity paradox and eruptive variables like FUors and EXors may represent an important stage of the secular evolution protostars, suggested to represent a transition between the Class I and Class II phases (e.g. Hartmann et al. 1998; Dunham & Vorobyov 2012).

**The “luminosity problem” and the role of eruptive variables:** Mass accretion in low mass protostars has recently come to focus as an increasing number of studies show that the traditional models of an inside-out collapse has difficulties explaining the variety of mass accretion rates seen in different star-

forming systems. A sizable fraction of young objects appear to be underluminous and the identification of this population has given support to the arguments of the so-called luminosity problem. The average accretion luminosity observed in embedded protostars is around  $2 L_{\odot}$  (Enoch et al. 2009), however the expected average accretion luminosity released due to the gravitational energy would have to be  $\approx 3$  times higher. This factor would be even higher if one takes into account the expected increase in the luminosity of the central source towards the Class I phase. The proposed solution to this problem is that accretion onto protostars is predominantly variable, as proposed early on by Hartmann et al. (1998). In this episodic accretion paradigm, early protostellar phases exhibit repetitive bursts of high accretion rates (up to  $10^{-4} M_{\odot} \text{ yr}^{-1}$ ), during which a sizable fraction of the final stellar mass is assembled. Burst phases are short-lived and are followed by long, quiescent periods where accretion rates drop by at least 2-3 orders of magnitude.

**HL Tau:** Disks around Class II sources have been subject of intense scrutiny, being identified as the possible locations where planets form. However many studies suggested that the mass content of protoplanetary disks is not sufficient to form the distribution of planetary masses observed in many systems of exoplanets (Miotello et al. 2018). With the advent of Atacama Large Millimeter/submillimeter Array

(ALMA) and once the first long-baseline campaign observations were made available, an unexpected and controversial result questioned our understanding on the formation of stars and planets. The observations resolved the disk of just a one-million year old protostar (thus a Class I source) (HL Tau, ALMA Partnership et al. 2015) revealing a series of gaps which *suggested that planets form synchronously with protostars and not later, as it has long been theorized*. While the interpretation of the ALMA observations is still subject of an intense debate, follow-up studies of the gas distribution (Yen et al. 2016) and larger dust grains (Carrasco-González et al. 2016) seem to firmly establish the early planet formation scenario. Recent surveys of embedded YSOs find that disks indeed form very early (Tobin et al. 2020) while a survey of protoplanetary disk sources (Andrews et al. 2018) at high resolution reveals that disk gaps are the norm rather than the exception. The morphology for most of protoplanetary disks reveals that they are thin (as a result of dynamically settling the heavier dust particles toward the disk midplane) and the observed frequency of gaps suggests that planet migration or other dynamical effects that would result in large-scale disturbances are rather rare. The HL-Tau, disk sharing the same characteristics, places an upper limit for the formation of planets to one million years - unless the formation scales are revised.

### 3. Current developments and future perspectives

The obvious next step after the discovery of multiple gaps carved out in protoplanetary disks that indicate locations where planets form, would be to detect the planetary embryos themselves. Just a few years after HL Tau, SPHERE observations with VLT revealed an accreting planet embedded in the protoplanetary disk of PDS70, a Class II object with an estimated age of 5 Myr. A second planetary companion (PDS 70c) was discovered in 2019 using the VLT's MUSE. The discovery signifies the dawn of a new field where planets can be studied in-situ during their formation and as an expected result, many projects are currently scanning across known Class II disks aiming to directly image planets embedded in their natal disks.

New classes of objects are emerging as data of higher sensitivity, spatial and spectral resolutions become available from new generations of instruments, The PACS Bright Red sources (or PBRs for short) first identified about 10 years ago with the Herschel Space Observatory appear to represent an early YSO phase that has distinct physical characteristics rendering this group of objects a possible distinct class. At the same time, surveys of complex organic molecules around a specific subclass of embedded YSO, the so called "hot corinos" (Jørgensen et al. 2020), reveals possible indicators for a chemical evolution of these objects which can provide additional refinements on their evolution. More than independent chronometers, the study of the chemical composition of envelopes is important as it represents the starting point for the accretion of primordial atmospheres to young planets. Such studies can then provide comparisons of the relative abundances of complex organic molecules to the composition of meteorites, which gives us the opportunity to gain insights on the early formation of the solar system. Moreover, large surveys aiming to identify disks around embedded YSOs (Tobin et al. 2019) bring new insights on the disk demographics and morphology at the earlier development stages of YSOs, where planets are expected to start forming but also on the connection of these accretion structures to the protostellar envelopes. Finally, the new generation of

instruments currently in development or commissioning (e.g. ELT, JWST) are expected to provide new detailed insights in the processes governing the formation of stars and planets.

The relationship between these new classes of objects that bear distinct observational characteristics is currently being investigated. Hot corinos appear to strongly correlate with PBRs, identifying a new, extremely young class of YSO where the primordial ices covering the dust grains in their envelopes are heated for the first time, releasing complex organic molecules similar to the primordial material trapped in the cometary ices of our own solar system. Compared to the standard classification criteria, the new emerging classes can describe more accurately the transformations taking place during the formation of YSOs. It is worth repeating, for comparison, that the criterion differentiating between Class 0 and I sources is whether the central source has accumulated less - or more - that 50% of the envelope mass; however the mass of the emerging YSO can be only indirectly estimated, while the envelope mass is prone to large uncertainties.

The current classification schemes that rely solely on a limited set of dust properties of the surrounding disk and envelope cannot provide an accurate description of the multitude of processes that regulate the formation timescales. Star formation is driven by the interplay between the central source, the envelope, the disk and the ejecta (jets and outflows). All components are closely linked to each other through feedback processes, so that the evolution of protostars can only be placed into context by understanding the simultaneous co-evolution of each structural component.

Today, we have in hand significantly higher quality and much larger volumes of data, more advanced computing methods and higher computing power, which allow us to revisit the standard star-formation paradigm and in particular the evolutionary scheme of young stars and planets, using new machine learning techniques applicable to big data. To this end, support vector machines can identify hyperplanes on multidimensional spaces, providing us with more accurate and unbiased YSO classes. The photometric measurements employed in SED of-

ten collapse and average emission corresponding to different components and excited through different processes. Some of the most sophisticated ML codes available today have been developed aiming on image analysis and pattern recognition (e.g. PyTorch from Meta/Facebook and Google/Vision). Such codes are now used for a direct analysis of the original imaging or spectroscopic data of YSOs, extracting and efficiently organizing much more information from the available data. Self organizing maps are currently employed to explore the morphological classifications of YSO, providing new unbiased and rapid taxonomies on large datasets. Machine learning applications provide seemingly endless possibilities in a rapidly growing field. Unsupervised machine learning techniques such as deep learning can explore multi-dimensional data spaces searching for patterns and correlations with minimum human intervention. Such methods have the power to uncover the inner, unseen mechanisms that govern the formation of stars and planets. In this context NEMESIS<sup>2</sup> represents one of the largest, coordinated efforts to bring big data and machine learning techniques to revisit the formation and evolution of young stellar objects. NEMESIS aims to readjust the current classification scheme and its characteristic timescales so that it is concurrent with the most recent observational and theoretical constraints. To meet these goals NEMESIS is compiling the largest, panchromatic dataset comprising of all young stellar objects in nearby star-forming regions, harnessing critical information that resides in data from space missions. It will reprocess and analyze this unique dataset with supervised and unsupervised machine learning algorithms, deep learning neural networks for object detection, clustering and regression analysis of images in order to advance the analysis and interpretation beyond the current state-of-the-art. Ultimately, NEMESIS brings big data techniques and hybrid machine learning methods to systematically analyze and interpret

2. Novel Evolutionary Model for the Early stages of Stars with Intelligent Systems (<https://nemesis.univie.ac.at>) - This project has received funding from the European Union's Horizon 2020 research and innovation programme under grant agreement No. 101004141/

large data volumes in order to answer some of the most persisting questions, paving the path toward data intensive science applications in modern astrophysics.

### List of acronyms

<b>ALMA</b>	Atacama Large Millimeter/submillimeter Array
<b>CAI</b>	calcium-aluminium-rich inclusion
<b>EXor</b>	EX Lupi-type object
<b>FUor</b>	FU Ori-type object
<b>SED</b>	Spectral Energy Distribution
<b>YSO</b>	Young Stellar Objects

## References

- ALMA Partnership, Brogan, C. L., Pérez, L. M., et al. 2015, *Astrophysical Journal Letters*, **808**, L3
- Andre, P., Ward-Thompson, D., & Barsony, M. 1993, *Astrophysical Journal*, **406**, 122
- Andrews, S. M., Huang, J., Pérez, L. M., et al. 2018, *Astrophysical Journal Letters*, **869**, L41
- Apai, D. A. & Lauretta, D. S. 2010, *Protoplanetary Dust: Astrophysical and Cosmochemical Perspectives*
- Bontemps, S., Andre, P., Terebey, S., & Cabrit, S. 1996, *Astronomy & Astrophysics*, **311**, 858
- Carrasco-González, C., Henning, T., Chandler, C. J., et al. 2016, *Astrophysical Journal Letters*, **821**, L16
- Connelly, J. N., Bizzarro, M., Krot, A. N., et al. 2012, *Science*, **338**, 651
- Dionatos, O., Nisini, B., Codella, C., & Giannini, T. 2010, *Astronomy & Astrophysics*, **523**, A29
- Dunham, M. M., Stutz, A. M., Allen, L. E., et al. 2014, *Protostars and Planets VI*, 195
- Dunham, M. M. & Vorobyov, E. I. 2012, *Astrophysical Journal*, **747**, 52
- Enoch, M. L., Evans, II, N. J., Sargent, A. I., & Glenn, J. 2009, *Astrophysical Journal*, **692**, 973
- Evans, II, N. J., Dunham, M. M., Jørgensen, J. K., et al. 2009, *Astrophysical Journal Supplements*, **181**, 321
- Greene, T. P., Wilking, B. A., Andre, P., Young, E. T., & Lada, C. J. 1994, *Astrophysical Journal*, **434**, 614
- Hartmann, L., Calvet, N., Gullbring, E., & D'Alessio, P. 1998, *Astrophysical Journal*, **495**, 385
- Jørgensen, J. K., Belloche, A., & Garrod, R. T. 2020, *Annual Review of Astronomy & Astrophysics*, **58**, 727
- Kenyon, S. J. & Hartmann, L. W. 1990, *Astrophysical Journal*, **349**, 197
- Lada, C. J. 1987, in *IAU Symposium, Vol. 115, Star Forming Regions*, ed. M. Peimbert & J. Jugaku, 1–17
- Ladd, E. F., Adams, F. C., Casey, S., et al. 1991, *Astrophysical Journal*, **366**, 203
- Manara, C. F., Fedele, D., Herczeg, G. J., & Teixeira, P. S. 2016, *Astronomy & Astrophysics*, **585**, A136
- Miotello, A., Facchini, S., van Dishoeck, E. F., & Bruderer, S. 2018, *Astronomy & Astrophysics*, **619**, A113
- Myers, P. C. & Ladd, E. F. 1993, *Astrophysical Journal Letters*, **413**, L47
- Rigliaco, E., Natta, A., Testi, L., et al. 2012, *Astronomy & Astrophysics*, **548**, A56
- Rigliaco, E., Pascucci, I., Duchene, G., et al. 2015, *Astrophysical Journal*, **801**, 31
- Shu, F. H., Adams, F. C., & Lizano, S. 1987, *Annual Review of Astronomy & Astrophysics*, **25**, 23
- Stahler, S. W. & Palla, F. 2004, *The Formation of Stars*
- Tobin, J. J., Megeath, S. T., van't Hoff, M., et al. 2019, *Astrophysical Journal*, **886**, 6
- Tobin, J. J., Sheehan, P., Megeath, S. T., et al. 2020, *arXiv e-prints*, arXiv:2001.04468
- Wakita, S., Matsumoto, Y., Oshino, S., & Hasegawa, Y. 2017, *Astrophysical Journal*, **834**, 125
- Yen, H.-W., Liu, H. B., Gu, P.-G., et al. 2016, *Astrophysical Journal Letters*, **820**, L25



## Visit our website

<http://www.helas.gr>

The above web server contains information, both in greek and english, about the Hellenic Astronomical Society (Hel.A.S.), the major organization of professional astronomers in Greece. The Society was established in 1993, it has more than 250 members, and it follows the usual structure of most modern scientific societies. The web pages provide information and pointers to astronomy related material, useful to both professional and amateur astronomers in Greece. It contains a directory of all members of the Society, as well as an archive of all material published by the Society, including electronic newsletters, past issues of "Hipparchos", and proceedings of Conferences of Hel.A.S. The server is currently hosted by the University of Thessaloniki.

# Historical developments

by George Contopoulos

Academician and Honorary President of Hel.A.S.,  
Research Center for Astronomy and Applied Mathematics of the Academy of Athens

*I describe the historical developments of two fields of research where I was personally involved. These fields are (a) The existence of closed invariant KAM curves that secure the stability of linearly stable periodic orbits and (b) The bifurcations of periodic orbits.*

## 1. Existence of closed invariant KAM curves

The existence of closed invariant curves around a linearly stable invariant point of a 2D mapping was proved by Kolmogorov (1954), Arnold (1961, 1963) and Moser (1962). This is the well known KAM theorem. It is remarkable that Birkhoff (1927) did not believe in the existence of closed invariant curves and considered the linearly stable points to be in general unstable. Thus, the KAM theorem was a real breakthrough. However there have been doubts about it. In particular Dr. J. Bartlett made extensive numerical calculations of fixed points and invariant curves in the mapping

$$x' = x + \alpha(y - y^3), \quad y' = y - \alpha(x' - x'^3).$$

and found many cases where the invariant curves extend to infinity. Thus he argued that there are no closed invariant curves around the central periodic orbit, but all the curves that looked like closed were in fact tight spirals that proceeded gradually outwards.

He wrote me about his results on 15-4-76 and sent me a preprint of his paper "Instability of an area preserving polynomial mapping". He wrote me "I'm sending copies to Moser, Arnold and Hénon, among others. Moser thought (in November 1975) that I would find invariant closed curves if I went toward the origin, but I didn't. His theorem is not applicable to this mapping, even though he thought it was. I don't know where it is applicable, and suspect that it may fail for open dynamical systems (where particles can go to infinity). In any case, something is fishy, and it is not so with my work, which relies on simple continuity arguments".

These remarks could not be disposed off lightly. In fact, Bartlett was the first to study numerically, in a systematic way, the invariant curves formed by successive iterations of points around period-

ic orbits.

Thus, I replied to him (28-6-76) "Your paper is a very interesting and challenging one. However, I cannot agree with your conclusions. I think that your main argument is in p.17, 'If the fixed point is hyperbolic for a large value of  $\alpha$  and connected to infinity by its eigencurves, and if it remains hyperbolic through the shrinkage, then the eigencurves still exist and go to infinity, though the fixed point gets arbitrarily close to the origin as  $\alpha$  approaches its minimum value'. I do not think that this is established. After all there is a continuity between hyperbolas and ellipses, and no one expects the ellipses to go to infinity". Then I added "I expect that the outermost "closed" curves may not be really closed, but the inner curves probably are".

In another letter (18-12-76), I pointed to him that his statement that "the eigencurves still exist and go to infinity, though the fixed point gets arbitrarily close to the origin" is wrong.

Responding to my letters Bartlett changed a little his paper but insisted that if the eigencurves from a periodic orbit escape for a value of the parameter  $\alpha$  they continue to escape for smaller values of  $\alpha$  as long as the periodic orbit remains unstable. He only accepted that as  $\alpha$  decreases "a given region requires more and more mappings to escape".

This exchange of letters involved also M. Hénon, who sent a letter (10-2-77) to Dr. Bartlett where he pointed out that the number of mappings required for escape may go to infinity as  $\alpha$  decreases and reaches a critical value  $\alpha_c$ . Below this critical value  $\alpha_c$  the iterates of the various points close to the origin never escape, Hénon concluded "you seem to have been victim of a modern version of the 'Achilles and the tortoise' paradox". Hénon and I happened to be the referees of the paper of Bartlett. But while

we both agreed that Bartlett was wrong, we disagreed in our conclusion. I could not recommend publication of his paper, while Hénon wrote "it would be unfair for the referee to use his privileged position to make his point of view prevail; and the best way to find the truth is to put the problem to a larger audience, i.e. to publish the controversial paper" (10-2-77). I then wrote to Bartlett (8-3-77) that I quite agreed with the objections of Hénon and suggested: "with all the experience that you have you should be able to estimate, at least roughly, the limiting value  $\alpha_c$ ".

The exchange of letters continued until 28-2-78, when Bartlett sent me a "final" version of his paper, where he had added a "Remark", stating: "The unresolved questions from our study are (1) if, for a given mapping, escape to infinity can occur, then do all eigencurves terminate at infinity? (2) If escape can occur for large values of  $\alpha$ , how could a decrease of  $\alpha$  bring about a transition to confinement of the eigencurves to within a bounded region?". He concluded that "both these questions may require further investigation".

After that I sent a letter to the Editor, accepting the paper for publication, and the paper was published in *Celestial Mechanics* (Bartlett 1978).

A few years later (1986) I invited Bartlett to a Florida Workshop on "Chaotic Phenomena in Astrophysics" and he presented a paper on the "Stability of an Area Preserving Mapping". In this paper he calculated the limits of the "almost stable" regions around the origin for various values of the perturbation  $\alpha$ . This was essentially what I was asking him to do in my 1976-77 letters. This paper was then published in the *Annals of the New York Academy of Sciences* 497, 78, 1987.

Bartlett wrote me in December 1987: "As I wrote previously, I can now locate nu-

merically the “KAM curves” associated with the Hénon-Heiles cubic mapping. This is now being done for large distances from the origin...”. Later Bartlett published the details of his calculations in *Celestial Mechanics and Dynamical Astronomy* (Bartlett 1989). In the acknowledgements he writes the following “The author wishes to thank G. Contopoulos for a stimulating discussion on October 7, 1987(sic), which provided the impetus

for the close examination leading to the present results”.

Thus, in the end Bartlett not only agreed with Hénon and me, but he was the first to find numerically the limiting value of the perturbation  $\alpha_c$ , below which we have closed invariant curves (KAM curves) around the central periodic orbit.



## References

- Arnold, V.I.: 1961, *Sov. Math. Dokl.* 2, 245  
 Arnold, V.I.: 1963, *Russ. Math. Surv.* 18 (5), 9; (6), 91  
 Bartlett, J.H.: 1978, *Celest. Mech.* 17, 3  
 Bartlett, J.H.: 1989, *Celest. Mech.* 46, 129  
 Birkhoff, G.D.: 1927, “Dynamical Systems”, *Amer. Math. Soc.*, Providence, R.I  
 Kolmogorov, A.N.: 1954, *Dokl. Akad. Nauk. SSSR* 98, 527  
 Moser, J.: 1962, *Nachr. Acad. Wiss. Göttingen II. Math. Phys. Kl.* 1

## 2. Infinite Bifurcations

The appearance of infinite bifurcations of periodic orbits in dynamical systems is an important phenomenon because it leads to a large degree of chaos.

Consider periodic orbits in a system of two degrees of freedom. The main types of bifurcations in conservative systems were set up by Hénon (1965). These were supplemented with the resonant bifurcation types by Contopoulos (1970). A discussion of the various types of bifurcations is given in the book “Order and Chaos in Dynamical Astronomy” (Contopoulos 2002).

A given family of stable periodic orbits gives rise to an infinity of higher order bifurcating families. As the perturbation parameter  $\epsilon$  (e.g. the energy) changes, the rotation number (rot) of the periodic orbit changes continuously, and whenever it goes through a rational number there is a bifurcation of a resonant family of periodic orbits. However, the most important bifurcations appear when  $rot = 1/2$  or  $rot = 1$ .

When  $rot$  becomes equal to  $rot = 1/2$  the original periodic orbit becomes unstable, generating a stable bifurcating family of double period, and when  $rot = 1$  the periodic orbit becomes unstable, generating a stable bifurcating family of equal period.

I did a systematic numerical study of the bifurcations of periodic orbit in 1968, using the computers of the Institute for Space Studies and of Harvard University (Contopoulos 1970). In particular I found that the bifurcating families also undergo higher order bifurcations of equal and double period. These are called pitchfork bifurcations. I noticed that the intervals between successive bifurcations decrease as the perturbation increases. In a later paper (Contopoulos 1973) I presented a figure (Fig. 1) giving the stability index (the trace of

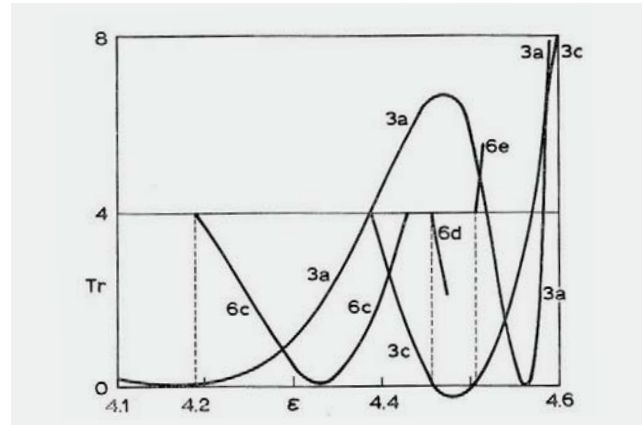


Figure 1: The stability index (trace) versus the perturbation  $\epsilon$  in a particular dynamical problem.

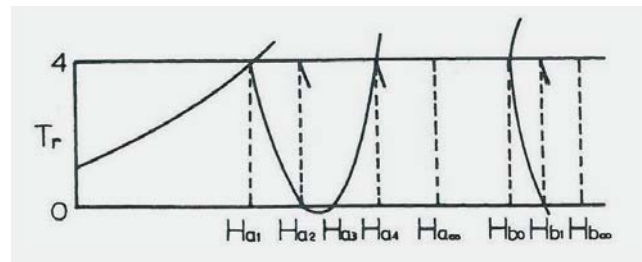


Figure 2: Successive bifurcations of periodic orbits. We give the trace of the monodromy matrix as a function of the energy  $H$ . The orbits are stable if  $0 < Tr < 4$ .

the monodromy matrix) as a function of the perturbation. In this figure I mark the bifurcations of double and equal period at the successive transitions to instability of the bifurcating families. I indicated that there seem to be infinite pitchfork bifurcating families, and all bifurcating families become eventually unstable after a critical value of the perturbation  $\epsilon_c$ . However, for even larger values of  $\epsilon$  we have new sets of bifurcating families. These families are called irregular, because they are not connected with the original family that starts at  $\epsilon = 0$ .

In another paper (Contopoulos 1975) I gave a schematic figure (Fig. 2) where I indicate the termination of the infinite bifurcations from the original family,  $H_{a\infty}$ , and from the new (irregular) families  $H_{b\infty}$ , etc.

Then I wrote “The question remains open whether there is an upper limit of

the values  $H_{a\infty}, H_{b\infty}, \dots$  beyond which all periodic orbits are unstable”.

On this subject I had an exchange of letters with J. Ford in 1979. Joe Ford wrote me (2 April '79) “Following Poincaré and Birkhoff, you have called attention to the fact that the stability of a periodic orbit is inherited but never closed. Numerical work by John Greene however indicated that there might be chaotic phase space regions in which there appear no stable periodic orbits at all...”. In order to resolve this seeming paradox, John Greene then conjectured that, as some system parameter varies, the infinite bifurcation sequence (in which the stability is inherited) might complete its run... As a consequence, beyond some critical value of this system parameter, there could indeed be no stable periodic orbits at all”. He then gave an example of such a behavior and asked my opinion. I replied on 10 April '79, giving essentially the

same remarks as in my 1975 paper. I gave then as an example the case of the logistic map  $x_{n+1} = ax_n(1-x_n)$  provided by May (1976) where new sets of stable families, like the families beyond  $H_{b0}$  of the above figure, appear all the way up to the limit of the chaotic region at  $a=4$ . Much later we emphasized the role of stable periodic orbits in providing recurrence of order in chaos (Contopoulos et al. 2005). Namely in the case of the standard map it was shown analytically that there are intervals of stability for arbitrarily large perturbations. Thus, there is no upper limit of the perturbation beyond which chaos is complete. After my papers of 1970, 1973 and 1975 many people studied the bifurcations of periodic orbits in dissipative and conservative systems, Feigenbaum (1978, 1979) and Couillet and Tresser (1978) found, independently, that the "bifurcation ratio" (i.e. the ratio between successive intervals between successive bifurcations) tends to a universal number  $\delta=4.67$  as the bifurcation order tends to infinity. This ratio had been found already by Grossman and Tomae (1977) but they did not state its universal character. By universal we mean that it is the same for all systems that have a quadratic maximum in the rotation curve (that gives *rot* as a function of the perturbation, or the energy). If the maximum is not quadratic one may find different ratios (de Souza-Vieira, Lazo and Tsallis, 1987). On the other hand, I found (1979) examples of families that had infinite intervals of stability and instability decreasing with a ratio  $\delta$ . In a particular case of two oscillators  $q_1$  and  $q_2$  of equal period coupled by a term  $q$ ,  $q_2^2$  it was  $\delta=9.22$  (Contopoulos and Zikides 1980). At every transition to instability we had a bifurcation of equal or double period family. In the limit, after infinite bifur-

cations of this type the periodic orbit led to an escape orbit. Later we found more cases of infinite equal and double period bifurcations along the same family leading to escapes. The existence of infinite transitions to instability was proven by Churchill, Pecelli and Rod (1979, 1980).

Then Heggie (1983) found analytically that in such cases the bifurcation ratio  $\delta$  is not universal, but depends on the potential. E.g. in our case the ratio  $\delta=9.22$  is equal to  $\delta = \exp(\pi\sqrt{2})$ .

On the other hand, Benettin, Cercignani, Galgani and Giorgilli (1980) found the bifurcation ratio for period doubling bifurcations in conservative systems that was equal to  $\delta=8.72$ . They noticed that this number was quite different from the corresponding ratio for dissipative systems  $\delta=4.67$  and close to the value  $\delta=9.22$  found by Contopoulos and Zikides (1980). However, it was established later that the ratio  $\delta=8.72$  of periodic doubling bifurcations for conservative systems is also universal, while the ratio  $\delta=9.22$  for bifurcations of the same family (leading to its instability or stability) is not universal (it is different in other dynamical systems). I had an exchange of letters about bifurcations with Galgani, Giorgilli, Rod and Ford starting in 1979. Galgani wrote me on 21-9-79: "You already had cases of successive bifurcations of the type (Fig. 2). You should find  $|E_n - E_\infty| = \sigma^n$ . Moreover the number  $\alpha$  should be "largely" independent of the potential. Try to check it".

I did check it with the data of my 1970 paper and I found the number 8.72, which was the bifurcation ratio for conservative systems.

Then I organized a meeting in 1980 in ESO (at CERN, Geneva) on "Bifurcations in Dynamical Systems". Among the par-

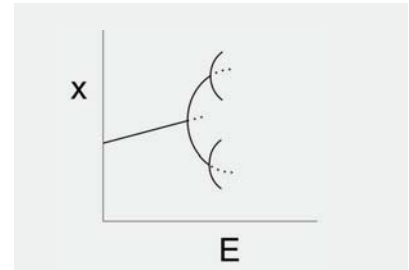


**Figure 3:** Successive period doubling bifurcations. The position  $x$  of the periodic orbits is given as a function of the energy,  $E$  (—) stable, (---) unstable orbits.

ticipants were Drs. Greene, Eckmann, Couillet, Galgani, Giorgilli, Benettin, Martinet, etc. I spoke about my recent results on infinite bifurcations. Later Drs. Greene, MacKay, Vivaldi and Feigenbaum (1981) published a paper on bifurcations in conservative systems, where they write "Conversations and communications with Dr (...) Contopoulos have contributed greatly to this paper". It was then clear that there are two universal numbers for period doubling bifurcations,  $\delta=4.67$  for dissipative systems and  $\delta=8.72$  for conservative systems.

I had also a correspondence with D.L. Rod on infinite bifurcations in 1980. Dr. Rod wrote to me on 16 May '80: "I hope you will keep us informed of your interesting research in this area. The careful diagrams you have plotted are of immense use to mathematicians in trying to unravel the story of stochasticity".

Another aspect of the problem of infinite pitchfork bifurcations was the appearance, in some cases, of inverse pitchfork bifurcations that led to a joining of the successive bifurcating families, so that finally only the original family remained, which became stable (Contopoulos 1983). In this way an infinity of bubbles was formed. Further work on this subject was done by Oppo and Politi (1984), Bier and Bountis (1984), Stone (1993) and others, that refer to my work.

## References

- Benettin, G., Cercignani, C., Galgani, L. and Giorgilli, A.: 1980, *Lett. Nuovo Cim.* 28, 1
- Bier, M. and Bountis, T.C.: 1984, *Phys. Lett. A* 104, 239
- Churchill, R.C., Pecelli, G. and Rod, D.L.: 1979, *Lecture Notes in Physics* 93, 76
- Churchill, R.C., Pecelli, G. and Rod, D.L.: 1980, *Rat. Mech. and Anal.* 73, 313
- Contopoulos, G.: 1970 *Astron. J.* 75, 108
- Contopoulos, G.: 1973 in Tapley, B.O. and Szebehely, V. (eds) "Advances in Dynamical Astronomy", Reidel, Dordrecht, 177
- Contopoulos, G.: 1975 *IAU Symp.* 69, 209
- Contopoulos, G.: 1983 *Lett. Nuovo Cim.* 37, 149
- Contopoulos, G.: 2002 "Order and Chaos in Dynamical Astronomy", Springer, Berlin
- Contopoulos, G. and Zikides, M.: 1980, *Astron. Astrophys.* 90, 198
- Contopoulos, G., Harsoula, M., Dvorak, R. and Freistetter, F.: 2005, *Int. J. Bif. Chaos* 15, 2865
- Couillet, P. and Tresser, C.: 1978, *J. Phys. Colloques* 39, C5-25
- de Sousa Vieira, M.C., Lazo, E., and Tsallis, C.: 1987, *Phys. Rev. A* 35, 945
- Feigenbaum, M.: 1978, *J. Stat. Phys.* 19, 25
- Feigenbaum, M.: 1979, *Lect. Not. Phys.* 93, 163
- Greene, J.M., MacKay, R.S., Vivaldi, F. and Feigenbaum, M.: 1981 *Physica D* 3, 468
- Grossman, S. and Thomaes, S.: 1977, *Z. Naturforschung* 32A, 1353
- Heggie, D.C.: 1983, *Celest. Mech. Dyn. Astron.* 29, 207
- Hénon, M.: 1965 *Ann. Astrophys.* 28, 992
- May, R. M.: 1976, *Nature* 261, 459
- Oppo, G.L. and Politi, A.: 1984, *Phys. Rev. A* 30, 435
- Stone, L.: 1993, *Nature* 365, 617

# COSPAR's 44<sup>th</sup> Scientific Assembly in Athens: a first for Greece at a historic juncture

by Manolis K. Georgoulis  
on behalf of the COSPAR Athens 2022 Local Organizing Committee  
COSPAR Athens 2022 LOC Chair - National Representative to COSPAR

The poster features a dark space background with a central illustration of a woman in a white dress holding a globe, surrounded by various planets and stars. In the top left corner, there is a COSPAR logo with a globe and the text 'COMMITTEE ON SPACE RESEARCH'. Below the logo, there is a silhouette of the Parthenon. The main text reads 'COSPAR 2022' in large white letters, followed by '44<sup>th</sup> SCIENTIFIC ASSEMBLY' and '16-24 July 2022, Athens, Greece' and 'Megaron Athens International Conference Centre'. A white box contains the text 'aMUSED by the Athenian URANIA'. At the bottom, the website 'www.cosparathens2022.org' is displayed in white.

## Online resources:

Local website of COSPAR Athens 2022: <https://www.cosparathens2022.org/>

Invitation to attend: <https://www.cosparathens2022.org/at-a-glance/invitation/>

COSPAR Athens 2022 candidacy video (full length): <https://www.youtube.com/watch?v=7BBC4CK-Nxg>

COSPAR Athens 2022 candidacy video (teaser): <https://www.youtube.com/watch?v=JBhB0ALUpE>

**A** nearly five-year endeavor undertaken by a team of 21 senior scientists, including astronomers, astrophysicists, space researchers, technologists, and aerospace medical professionals within Greece and in the Diaspora is coming to a profound culmination this summer, with the implementation of the 44<sup>th</sup> Scientific Assembly of the Committee on Space Research (COSPAR). Dreaming of a COSPAR Assembly in Greece at a time that Greece had only started emerging from an existential economic and social crisis, then preparing the candidacy folder, campaigning for and defending it before the COSPAR Council four years ahead of the envisioned Assembly's time and then going through all preparatory phases scholastically, until this stage –on the verge of the Assembly's actual occurrence– is an experience that will be staying with us

forever. A successful implementation of *COSPAR Athens 2022*, as the organization was coined early in the process, will showcase and solidify Greece's ability to organize events of global caliber in our broad fields of research. Indeed, one can think as only precedents the European Week of Astronomy and Space Science (EWASS) in July 2016 in Athens and the XVIII General Assembly of the International Astronomical Union (IAU) in August 1982 in Patras. Both earlier meetings were, arguably, somewhat smaller than COSPAR Athens 2022.

But what is COSPAR? The Committee on Space Research (<https://cosparhq.cnes.fr/>) was an offspring of the space age. Shortly after Sputnik's launch in 1957, the International Council of Scientific Unions, now known as the International Science Council, established its Com-

mittee on Space Research in 1958<sup>[1]</sup>. COSPAR's mission according to the latest *COSPAR Strategic Action Plan 2019 – 2023*<sup>[2]</sup> is to “assemble a worldwide community of scientists who are dedicated to international cooperation in space research”, free of any geopolitical impediments. Humanity saw the dawn of the space age at a time close to the peak of the Cold War, hence the need to promote space science in the interest of peace and global stability became pressing. It is interesting to mention that until the dissolution of the Soviet Union in the late 1980s – early 1990s, COSPAR had two Presidents: one from the East, typically the Soviet Union, and one from the West, typically Europe and the United States. This obsolete rule still bears an imprint on the present COSPAR structure, that now foresees a President and two Vice-Presidents.

COSPAR is a Committee of member states (i.e., national scientific institutions) and scientific unions. Figure 1 shows the COSPAR World, extending over all continents but Antarctica, with 45 member states. COSPAR also has 13 international scientific unions as members, including the IAU. Each country and union have one representative in the COSPAR Council, that is the executive body implementing all major decisions of the Committee. Deliberations during the Council Meetings are moderated by the COSPAR President, the two Vice Presidents, and the Secretariat, the latter consisting of the Executive Director, the Associate Director and the Administrative Coordinator. The COSPAR Secretariat is based in Paris, co-located with the French *National Centre of Space Research* (CNES). Remarkably, Greece was one of the early COSPAR members, forming a National Committee for Space Research within the Academy of Athens shortly after COSPAR's establishment, which forged a national membership that continues to this day.

COSPAR has an elaborate scientific structure<sup>[4]</sup> consisting of eight Scientific Commissions (A – H) spanning from Meteorology and Climate to Life Sciences, Material Sciences and Fundamental Physics in Space. It also features twelve Scientific Panels, spanning from Satellite Dynamics to Education and from Innovative Solutions to Social Sciences and Humanities. In addition, it has six Task Groups active on outstanding and pressing scientific problems. COSPAR has recently formed an Advisory Body, the *Committee on Industry Relations*,

comprising high-ranking representatives from the biggest national space organizations, as well as global aerospace industry players. Last but not least, COSPAR is active in publications, teaming up with Elsevier to create two peer-reviewed journals (the *Advances in Space Research* and *Life Sciences in Space Research*), a voluminous informational magazine (*Space Research Today*) and a vibrant electronic Newsletter<sup>[5]</sup>. This intense activity has led to cutting-edge roadmap studies<sup>[6]</sup> on terrestrial and space-related topics. More are in the works as these lines are written.

Among focused workshops, task group meetings and symposia, COSPAR's prime vehicle for pursuing its mission and objectives is its biennial Scientific Assemblies, organized in a different continent each time<sup>[7]</sup>. These Assemblies have been long recognized as top-tier events, showcasing the evolving state-of-the-art in space research and technology. All major space organizations and agencies are represented at high level in the Assemblies and participate in Round Tables, Latest Results sessions and press releases attended by an indiscriminate mosaic of global space scientists, typically in the thousands. COSPAR Assemblies have had their share of unforeseen adversities, almost exclusively in recent years, in spite of an overall smooth implementation since the first Assembly in London in 1958. The one and only COSPAR Assembly ever to be canceled was that of Istanbul, Turkey, in 2016: the major developments following an attempted *coup-d'état* in July of that year led to a diffi-

cult decision to cancel, less than two weeks before the Assembly's start. The Covid-19 pandemic in 2020 postponed the Assembly of Sydney, Australia, by 5 months, initially as a hybrid undertaking consisting of in-person and virtual participations. Hardening measures in Australia and several parts of the world finally led to a fully virtual Assembly in January 2021.

COSPAR Athens 2022 was selected to implement the 44<sup>th</sup> COSPAR Scientific Assembly during the Council Meeting of the 42<sup>nd</sup> Scientific Assembly in Pasadena, California, USA, in July 2018. Athens was competing among four strong European candidacies (the others were Lausanne, Prague, and Warsaw) and cleared its selection early in the process, collecting 55% of the total votes already in the first round. The candidacy, and subsequent COSPAR Athens 2022 organization, is coordinated by the National Committee of Space Research of the Academy of Athens and the newly established Hellenic Space Center (HSC; <https://hsc.gov.gr/>). The LOC also comprises four Greek scientists of the diaspora (three in the United States and one in France) – see complete list<sup>[8]</sup> at the end. Since its candidacy inception, COSPAR Athens 2022 enjoys the unwavering support of virtually all major Greek universities and prominent research centers, while written statements of support were submitted to COSPAR prior to the selection by a plethora of Greek public and private organizations. This support has culminated into several sponsorships from entities in Greece and abroad. Last, but

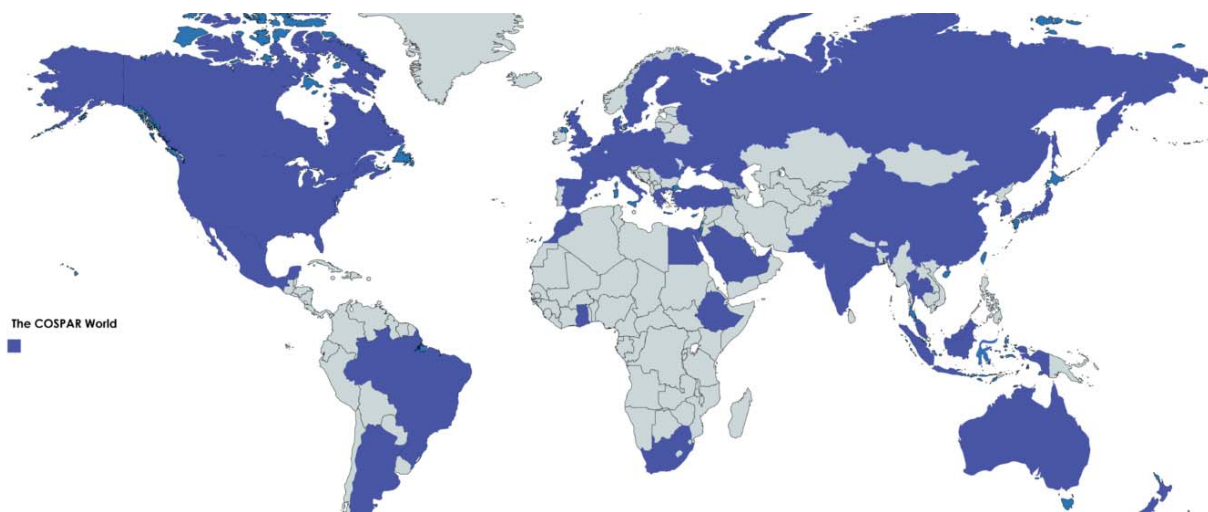
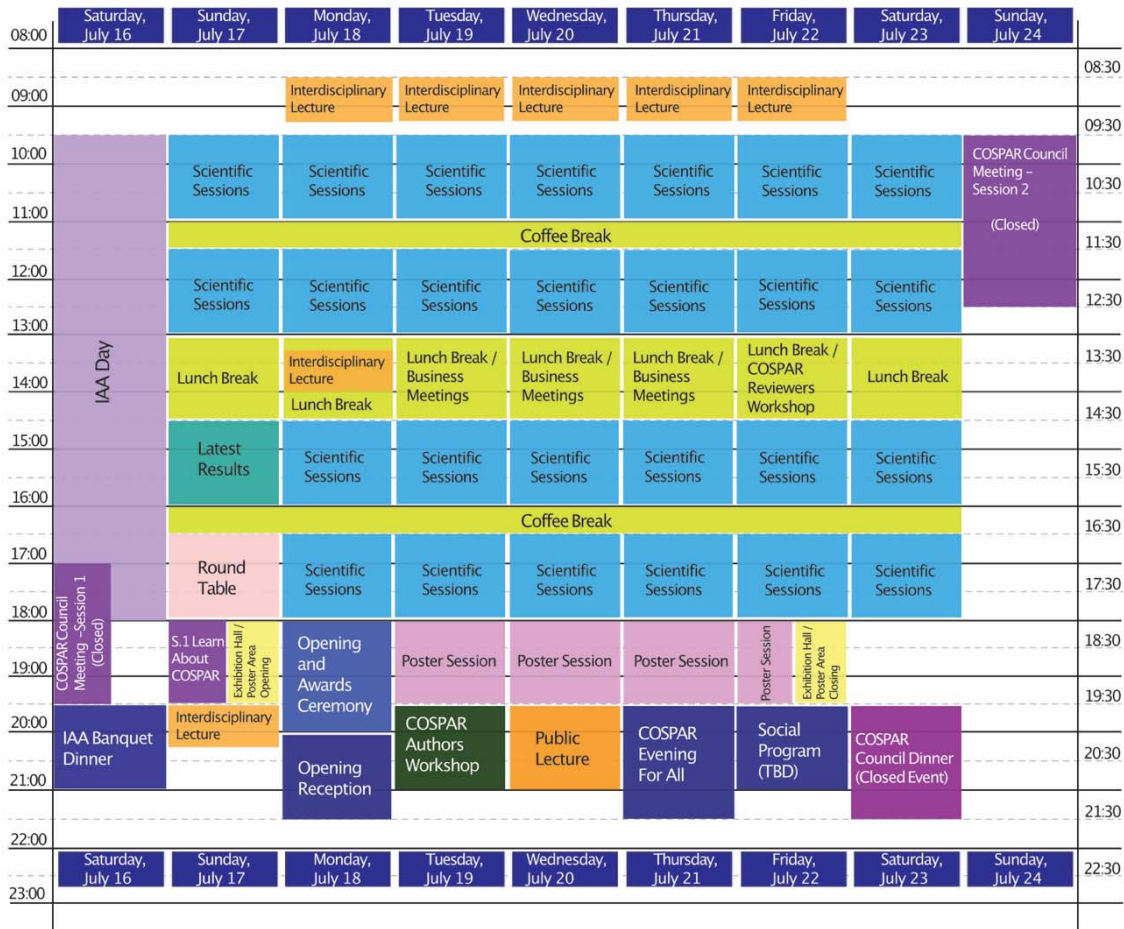


Figure 1. The COSPAR World, comprising countries shaded in blue, courtesy of COSPAR<sup>[3]</sup>.

certainly not least, an ‘army’ of 130+ volunteers have, in recent months, enthusiastically pledged their time and energy to support an elaborate Assembly structure, making sure that participants will always have somebody a few steps away to address their needs, or be there to provide help, if and when needed.

The nominal abstract submission deadline for COSPAR Athens 2022 expired in February 2022. The submission phase resulted in more than 3,500 submitted abstracts, distributed among a total of 144 approved scientific sessions over all Commissions, Panels and Task Groups. Facilitating this immense scientific

input requires a total of 30 parallel sessions for seven full meeting days (see the Program-at-a-Glance in Figure 2) and, even in this case, the time capacity is fulfilled at approx. 99.5%. Initially planning the Assembly at the Megaron Athens International Conference Center (MAICC), it soon became evident –also



**Figure 2.** COSPAR Athens 2022 Program-at-a-Glance, including scientific sessions and plenary Assembly functions. The Assembly is traditionally preceded by the daily convention of the International Academy of Astronautics (IAA Day), planned to take place at the Main Hall of the Academy of Athens’ headquarters.



**Figure 3.** (Left) The main COSPAR Athens 2022 venue, the Megaron Athens International Conference Center. (Right) The Headquarters Divani Caravel Hotel, sharing a significant load of the scientific program. The two venues are approx. 1 km apart and will be connected via a shuttle bus rotating every 20 – 30 minutes for the duration of the Assembly.

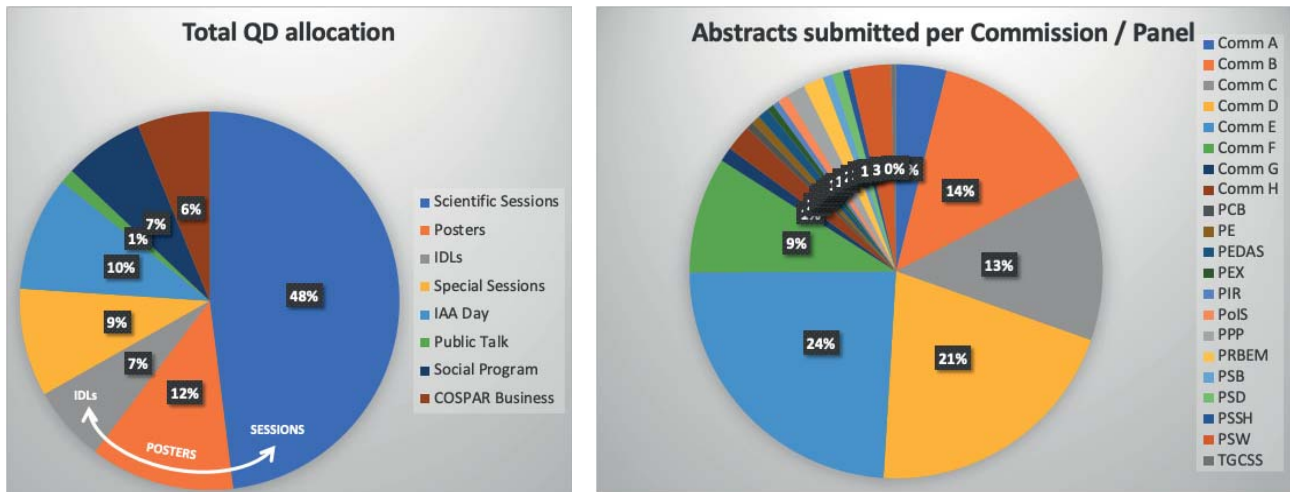


**Figure 4.** (Left) The time allocation of COSPAR Athens 2022 distributed among different functions and shown as a percentage of the total allocated quarter days (QDs: contiguous 90-min sessions). Scientific functions (oral sessions, poster sessions and interdisciplinary lectures [IDLs]) amount to 67% of the total time allocated. (Right) Percentage of the total number of abstracts submitted to different Commissions and Panels. The Commissions standing out are B (Moon / Planets); C (Atmospheres); D (Plasmas); E (Astrophysics) and F (Life Sciences), amounting to 81% of the total submitted abstracts.

in view of foreseen enhanced distancing measures— that a second venue should take part of the science program load. The venue of choice is the Divani Caravel Hotel (Figure 3), a 5-star facility serving as the Assembly's Headquarters Hotel, that will also host several of the Assembly's dignitaries.

As seen by the Program-at-a-Glance, COSPAR Athens 2022, like every COSPAR Assembly, hosts a variety of functions alongside the body of scientific sessions. A summary mix of these functions and their time allocation over the meeting, are shown in Figure 4 (left) while the fractions of abstracts over sessions of different Commissions and Panels are shown in Figure 4 (right). Figure 4 does not include the Assembly's Associated Events<sup>[11]</sup>, an array of diverse scientific functions facilitated either at lunch-time, due to the overall lack of vacant session rooms, or during the few empty room slots.

A vibrant exhibition area will be operating for most of the Assembly. This space allows for closer, more relaxed interaction between exhibitors and attendees, as well as better information on the various exhibits, organizations, and institutes participating. In this Assembly, the main pavilion will be occupied by the US National Aeronautics and Space Administration (NASA) and will be featuring the popular NASA Hyperwall<sup>[9]</sup> that serves as a magnet for occasional audience and the venue of several bonus

presentations and events. Also prominent will be the pavilions of the European Space Agency (ESA), the joint pavilion of the si-Cluster and the Hellenic Association of Space Industry (HASI) and that of the HSC. An assortment of smaller participations by key international labs and organizations will complement the exhibition part, while several more booths are being reserved as these lines are written.

Given the course of the Covid-19 pandemic over the past 2.5 years, numerous planning meetings were devoted to the Assembly's format. The prevailing view, that ultimately led to the decision, was that COSPAR Athens 2022 will be a hybrid event, but with the emphasis clearly placed on physical participation. All plenary sessions of the Assembly will be livestreamed for virtual participants, but not the regular session rooms, that would be infeasible cost-wise. This said, all functions included in the Assembly's Program-at-a-Glance will be recorded, edited for quality assurance and consistency, and made accessible to all participants within 36 hours from physical occurrence. Virtual speakers will upload their recorded presentations in a certain multimedia format adhering to well-defined specifications. These movies will be played back in their respective times in the program. Due to the lack of voice and picture interaction between virtual and in-person participants, there will be a chat wall operating continuously, different for each session, in which

questions and answers will be handled. This will be a custom function provided by COSPAR's ZARM contractor, in the framework of its cooperation with the COSPAR Athens 2022 LOC.

The above arrangements were dictated by today's planning ambiguity, enhanced by recent service fee spikes. The meeting experience will be complemented by two online applications: first, a platform dedicated to the meeting, where all recordings will eventually be stored, along with oral and poster presentation files. Second, a platform-free, Google Chrome-based Progressive Web App (PWA) that will provide all relevant meeting information, including the detailed Assembly program and abstracts. Both in-person and virtual participants will have access to both online facilities at will. The Speaker Ready area will be both physical (i.e., at the MAICC) and virtual, to allow every participant to view, edit and finalize their presentation files with an option to totally avoid the typical lines of the physical service. All in all, COSPAR Athens 2022 will be a 'traditional' COSPAR Assembly, of the ones the international community has come to appreciate and support, but adapted for the 21<sup>st</sup> century and its meeting and networking capabilities. The international community seem to appreciate this and aim to travel to Athens at an overwhelming majority.

A totally unforeseen development, namely, the war in Ukraine, has kept COSPAR and the COSPAR Athens 2022

organization alert. COSPAR swiftly offered a statement available prominently in its homepage<sup>[1]</sup> in which it fully aligns with its statutes and rich history of collaboration between the East and the West. COSPAR fully understands the detriment of scientific isolation and works to enable equal participation to all scientists, regardless of citizenship, on the condition of scientific-only exchange and a zero tolerance to propaganda. The COSPAR Athens 2022 LOC has strived to implement this principle by issuing, even before the war broke out, a Code of Conduct<sup>[10]</sup> that even foresees such situations. We hope that both affected countries will be able to send delegates to the meeting and we

are standing by to help them, facilitating their attendance and ultimately welcoming them to the Assembly's deliberations.

Unbeknownst to us when we campaigned and competed for the 2022 COSPAR Scientific Assembly, Greece is now called upon to organize a historic gathering, the first after humanity's slow and gradual transition from the Covid-19 to the post-Covid era. Perhaps more importantly, COSPAR Athens 2022 is the first Assembly organized within a greater European geographical swath in which war is, once again, a gruesome reality. We can only find it highly symbolic that this Assem-

bly is happening in Greece, the cradle of phenomenology, hypothesis, analysis and theory, all based on a solid foundation of the uncompromising scientific method. Embodying COSPAR's ideals and *modus operandi*, we believe in peace proliferating in frank and calm scientific exchanges and strive to provide this environment to all participants of the forthcoming Assembly. It is long overdue to showcase Greece's and its Diaspora's contemporary scientific standing in space science and research, alongside its hard-to-overstate classical contributions to philosophical debates rooted on a healthy, solid reasoning.

### COSPAR Athens 2022 Local Organizing Committee

**Chair, Scientific Program Committee (SPC):** Academician Dr. Stamatios M. Krimigis, *Greece*

**Chair, LOC:** Dr. Manolis K. Georgoulis, *RCAAM of the Academy of Athens, Greece*

**Vice Chair, SPC:** Prof. Ioannis Dagleis, *HSC and the University of Athens, Greece*

**Vice Chair, LOC:** Dr. Nick Sergis, *HSC, Greece*

Dr. Vassilis Angelopoulos, *University of California Los Angeles, USA*

Dr. Alceste Bonanos, *National Observatory of Athens, Greece*

Academician Prof. George Contopoulos, *Greece*

Dr. Athena Coustenis, *Observatoire de Paris-Meudon, LESIA/CNRS, France*

Dr. Manos Kitsonas, *Planetarium Director, Eugenides Foundation, Greece*

Dr. Haris Kontoes, *National Observatory of Athens and BEYOND Center of Excellence, Greece*

Dr. Chrysoula Kourtidou-Papadeli, *Director of IASI Aeromedical Center, Greece*

Prof. Chryssa Kouveliotou, *George Washington University, USA*

Prof. Nick Kylafis, *Emeritus, University of Crete, Greece*

Dr. Paul Michelis, *Institute of Mechanics of Materials and Geosciences, S.A., Greece*

Dr. Manolis Plionis, *Director, National Observatory of Athens, Greece*

Prof. Emmanuel T. Sarris, *Emeritus, University of Thrace, Greece*

Dr. Dionysis T. Simopoulos, *Emeritus Planetarium Director, Eugenides Foundation, Greece*

Prof. Kanaris Tsinganos, *Emeritus, University of Athens, Greece*

Prof. Loukas Vlahos, *Retired, University of Thessaloniki, Greece*

Dr. Angelos Vourlidis, *The Johns Hopkins University Applied Physics Laboratory, USA*

Academician Prof. Christos S. Zerefos, *Secretary General, Academy of Athens, Greece*

## References

[1] About COSPAR: <https://cosparhq.cnes.fr/about/>

[2] COSPAR Strategic Action Plan 2019–2023: <https://cosparhq.cnes.fr/about/cospar-strategy-statement/>

[3] COSPAR's National Scientific Institutions: <https://cosparhq.cnes.fr/about/members/national-scientific-institutions/>

[4] COSPAR Scientific Structure: <https://cosparhq.cnes.fr/scientific-structure/>

[5] COSPAR Publications: <https://cosparhq.cnes.fr/publications/>

[6] COSPAR Scientific Roadmaps: <https://cosparhq.cnes.fr/scientific-structure/cospar-scientific-roadmaps/>

[7] COSPAR's list of Scientific Assemblies: <https://cosparhq.cnes.fr/events/scientific-assemblies/>

[8] COSPAR Athens 2022 LOC: <https://www.cosparathens2022.org/committees/organizing-committee/>

[9] About NASA's Hyperwall: <https://eosps.nasa.gov/content/about-nasas-hyperwall>

[10] COSPAR Athens 2022 mission and objectives: [https://www.cosparathens2022.org/at-a-glance/mission-and-objectives/Code\\_of\\_Conduct](https://www.cosparathens2022.org/at-a-glance/mission-and-objectives/Code_of_Conduct) at [https://www.cosparathens2022.org/articlefiles/COSPAR\\_2022\\_Code\\_of\\_Conduct.pdf](https://www.cosparathens2022.org/articlefiles/COSPAR_2022_Code_of_Conduct.pdf)

[11] <https://www.cosparathens2022.org/program/associated-events/>

## Back issues of Hipparchos

Hipparchos is the official newsletter of the Hellenic Astronomical Society. It is distributed by post to the members of the society. You can download back issues from: <http://www.helas.gr/news.php>

